



Free-energy profiles along reduction pathways of MoS₂ M-edge and S-edge by dihydrogen: A first-principles study

Pierre-Yves Prodhomme^a, Pascal Raybaud^b, Hervé Toulhoat^{c,*}

^a Direction Chimie et Physico-Chimie Appliquées, IFP Energies nouvelles, 1 et 4 avenue de Bois-Préau, 92852 Rueil-Malmaison, France

^b Direction Catalyse et Séparation, IFP Energies nouvelles, Rond-point de l'échangeur de Solaize, BP 3, 69360 Solaize, France

^c Direction Scientifique, IFP Energies nouvelles, 1 et 4 avenue de Bois-Préau, 92852 Rueil-Malmaison, France

ARTICLE INFO

Article history:

Received 20 October 2010

Revised 14 March 2011

Accepted 20 March 2011

Available online 23 April 2011

Keywords:

Density functional theory

HDS catalysts activation

Free-energy surface phase diagrams

Dihydrogen activation

Brønsted–Evans–Polanyi relationships

Sulfur vacancies

SH and MoH surface groups vibrational

frequencies

ABSTRACT

We present the results of DFT calculations of free-energy profiles along the reaction pathways starting from 50% coverage of MoS₂ M-edge and 100% coverage of S-edge by sulfur, and leading to 37% coverage, i.e. creation of anionic vacancies, upon reduction by dihydrogen and production of H₂S. Significant entropic and enthalpic corrections to electronic energies are deduced from the sets of normal modes vibration frequencies computed for all stationary and transition states. On that basis, we revisit and discuss the surface phase diagrams for M- and S-edges as a function of temperature, H₂ partial pressure and H₂S/H₂ molar ratio, with respect to ranges of conditions relevant to industrial hydrotreating operations. We show that in such conditions, anionic vacancies on the M-edge, and surface SH groups on the M- and S-edges, may coexist at equilibrium. Moderate activation barriers connect stationary states along all paths explored.

© 2011 Elsevier Inc. All rights reserved.

1. Introduction

To face an ever growing global energy demand, and depleting conventional oil resources, heavier crudes are increasingly refined into fuels. Simultaneously, local and global environment preservation regulations drive increased hydrogen addition, together with sulfur and other hetero-atoms removal, to end up with cleaner fuels. As such critical upgrades are achieved by catalytic hydroprocessing under a H₂ + H₂S atmosphere at high pressure, improved catalysts involving transition metal sulfides (such as MoS₂ based active phases) are keys to meet the rising challenges. However, basic questions such as the nature of active sites and the mechanism of hydrogen activation remain so far much debated or unanswered [1–5]. Providing well quantified data on the thermodynamic stability and activation pathways of hydrogen on MoS₂ is of paramount importance for a better understanding of hydrodesulfurization mechanisms. Indeed, determining the hydrogenation state of the catalyst in HDS working conditions will help for a better control of the surface chemical species: coordinatively unsaturated metallic sites (CUS), hydride, sulfhydryl group, sulfur anions. Most of

these species are suspected to be involved in the elementary steps of HDS reactions [6]: reactant adsorption, monohydrogenation, hydrogenolysis, and sulfur-vacancy regeneration.

Since most industrial hydroprocessing catalysts are based on MoS₂ nanoparticles, and it is now well established that catalytic activity is localized at their “M-edge” and “S-edge” surfaces [5,7], we establish here through first-principles (DFT) calculations including for the first time thermal and entropic effects on the catalyst, the free-energy profiles of dihydrogen and hydrogen sulfide exchanges with such surfaces, including elementary steps of dissociative adsorption, associative desorption, and surface diffusion of bonded hydrogen. From previous works neglecting entropic contributions [4,8–11], no clear consensus emerges, regarding in particular the formation of sulfur vacancies and the nature and stability of hydrogen species at edges. For instance, Paul and Payen [9] found that sulfur-vacancy creations on S-edge and M-edge by H₂ to release H₂S, are very endothermic (1.31 eV for M-edge and 1.89 eV for S-edge), and kinetically difficult to achieve processes (1.47 eV for the “M-edge” and 2.10 eV for the “S-edge”). However, S vacancies were shown experimentally to be related to catalytic activity [12,13], presumably offering chemisorption sites to hetero-aromatics and other unsaturated hydrocarbons and hence lowering activation barriers for further hydrogenation and hydrogenolysis steps, as moreover described by numerous DFT

* Corresponding author. Address: IFP Energies nouvelles, 1 et 4 avenue de Bois-Préau, 92852 Rueil-Malmaison, France. Fax: +33 (0) 1 47 52 70 22.

E-mail address: herve.toulhoat@ifpenergiesnouvelles.fr (H. Toulhoat).

studies [1,14–16]. Therefore, the present work aims at re-investigating the H₂S associative desorption processes to assess not only the stability of S vacancies on MoS₂ edges but also the free-energy barriers to vacancies formation.

Also, according to some of these works, H coverage was assumed to be hardly thermodynamically stable for few configurations [16,10,9], but since hydrogen ad-atoms on edges are expected to be primarily involved in hydrogenation and hydrogenolysis of adsorbed sulfided hydrocarbons, the reaction pathways for H₂ adsorption and H diffusion are re-investigated on both M- and S-edges.

In the present study, details on our DFT simulations are given in Section 2.1. In order to assess the stability of the catalyst edges, a thermodynamic model has been set up and is presented in Section 2.2. Then, in Section 3.1, are first presented the results of the computations performed on the reaction pathways for H₂ dissociative adsorption and H₂S associative desorption along M-edge 50%S, S-edge 100%S, S-edge 87%S and S-edge 50%S. The surface phase diagrams for the S-edge and the M-edge derived from these pathways according to our thermodynamic model are then shown in Section 3.2. In Section 3.3, we compare the computed frequencies of normal modes of vibration for surface species to available experimental data, taking care to relate the conditions of measurement and preparation of the solids for the latter, to the predicted stable states according to our analysis. In this way, we did our best to look for crucial experimental evidence capable of invalidating our theoretical prediction. In Section 3.4, we underline Brønsted–Evans–Polanyi relationships (BEPR) emerging for the dissociative adsorption of H₂ and associative desorption of H₂S on or from the surfaces considered in Section 3.1. The discussion undertaken in Section 4 focuses on the one hand on the main differences between our phase diagrams and the former ones proposed [15,17,18], and on the other hand on the significance of our results with respect to the problem of activation by H₂ of MoS₂ based hydrotreating catalysts. Finally, our conclusions are presented in Section 5.

2. Methods

2.1. DFT calculations

The computations were carried out according to the density functional theory [19] with the Vienna ab initio simulation package (VASP) [20], within the generalized gradient approximation, using the PW91 functional [21,22], and the projector augmented waves method [23] to treat the ionic–electronic interaction. The electronic density was calculated with a 350 eV cutoff energy, 3 k points in the irreducible Brillouin zone [24], and a 0.1 eV electronic energy smearing. For ground states, the residual forces were set lower than 0.02 eV/Å. The nudged elastic band (NEB) method was used to find the reaction paths [25], followed by the climbing image method [26], and the dimer method [27] to find the transition states (TS). The TS consistencies were verified when the higher forces applied on atoms were lower than 0.02 eV/Å, and the normal mode of the dynamical matrix exhibited only one imaginary frequency. In order to save computation time for the normal modes computation, only hydrogen, sulfur, and molybdenum atoms positions above the gray plane in Fig. 1 were kept free (corresponding to 20 atoms in Fig. 1). All other atoms were frozen. Normal mode frequencies were not corrected for anharmonicity.

In order to estimate the charge carried by each atoms, a Bader analysis [28] was carried out on the electronic density computed with VASP (self-consistent calculations on the valence electronic density including 6 valence electrons per atom) thanks to the program established by Henkelman et al. from the University of Texas at Austin [29–31]. In this analysis, the net charge of one atom is the

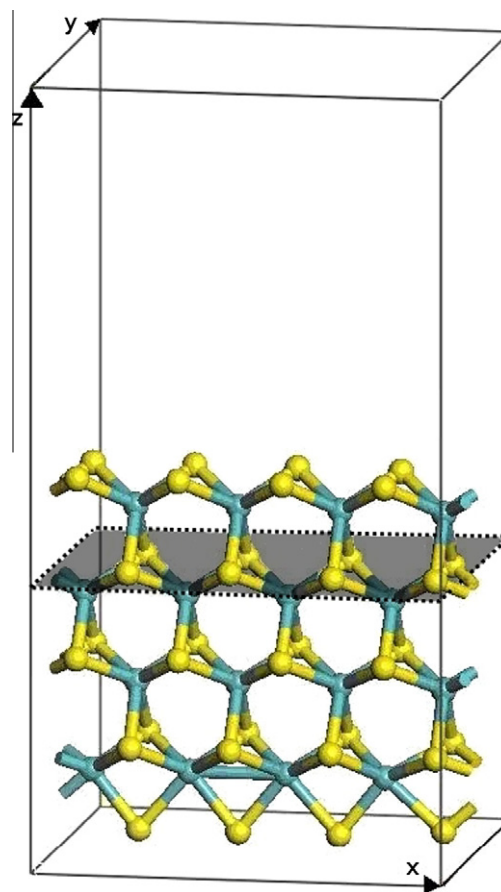


Fig. 1. A typical periodic slab model for MoS₂ S-edge, showing coverage by four S₂ bridges. Legend: (color on line) black spheres (turquoise): molybdenum atoms, gray spheres (yellow): sulfur atoms.

integral of the excess valence electronic density over the volume delimited by the zero-flux surface wrapping this atom minus 6e. On the zero-flux surface, the valence electronic density is minimal along the normal direction.

The parameters of the supercell, exhibited in Fig. 1, were similar to those previously used in Refs. [4] and [32]. Therefore, the model catalyst was composed of 4 Mo rows in the x-direction and 4 Mo rows in the z-direction. A 12.8 Å vacuum was allowed between each layer so that the slab was isolated in the y-direction. A single Mo row separated by 12.3 Å vacuum was considered in the y-direction, so that this layer was also isolated in this direction.

To find ground states, the simulated annealing method was applied, starting from the sulfur atoms on the edges in their bulk site. This heuristic method allows avoiding the system to become stranded in a local energy minimum. This simulated annealing procedure involved an ab initio molecular dynamics simulation on the Born–Oppenheimer surface, where the velocities were scaled every five steps, in order to reach after a while the targeted temperature. Between the rescaling steps the simulation was performed in the micro-canonical ensemble (constant N, V, E).

2.2. Thermodynamics corrections

The grand potential was computed in order to determine the most stable configurations. As the computed edges of the catalyst have all the same size, the grand potential was considered instead of the surface free energy:

$$\Omega(\mu_{\text{Mo}}, \mu_{\text{S}}, \mu_{\text{H}}) = E_{\text{MoS}_x\text{H}_y}^{\text{tot+vib}} - TS_{\text{MoS}_x\text{H}_y}^{\text{vib}} - n_{\text{Mo}}\mu_{\text{Mo}} - n_{\text{S}}\mu_{\text{S}} - n_{\text{H}}\mu_{\text{H}} \quad (1)$$

where $E_{\text{MoS}_x\text{H}_y}^{\text{tot}+\text{vib}}$ is the total DFT energy plus the vibrational enthalpy of the MoS_xH_y catalyst sheet containing n_S sulfur, n_{Mo} molybdenum, and with n_H hydrogens on the edge. $S_{\text{MoS}_x\text{H}_y}^{\text{vib}}$ is the vibrational entropy of MoS_xH_y . μ_{Mo} , μ_S and μ_H are the chemical potentials of molybdenum, sulfur and hydrogen respectively. This accurate approach including thermal and entropic effects on the catalytic phase is provided for the first time on these systems to our knowledge. The enthalpies and entropies of vibration were computed thanks to the usual relationships derived from statistical thermodynamics [33], using the normal modes of the atoms near to the edge, and assuming that the normal modes of the atoms below the first two layers at the edge do not change. It is remarkable that the vibrational part of the free energy is not a constant term for the catalyst along the reaction path (see Section 3). Hence for this reason, the phase diagrams (Figs. 11–13) have been computed for a set of temperatures representative of relevant HDS operations (473, 575 and 623 and 675 K).

As all the computed model catalysts contain the same number of Molybdenum atom, a curtailed grand potential is defined:

$$\Omega_c(\mu_S, \mu_H) = G_{\text{MoS}_x\text{H}_y} - n_S \mu_S - n_H \mu_H \quad (2)$$

where:

$$G_{\text{MoS}_x\text{H}_y} = E_{\text{MoS}_x\text{H}_y}^{\text{tot}+\text{vib}} - TS_{\text{MoS}_x\text{H}_y}^{\text{vib}} \quad (3)$$

At thermodynamic equilibrium, the chemical potential of an atom is the same in all phases. So the chemical potential of sulfur and the chemical potential of hydrogen are determined within the gas phase [34]:

$$\mu_S = \mu_{\text{H}_2\text{S}} - \mu_{\text{H}_2} \quad (4)$$

$$\mu_H = \frac{1}{2} \mu_{\text{H}_2} \quad (5)$$

Total energies plus vibrational ground state energies for H_2 and H_2S were computed at the DFT level, and the thermodynamic functions were calculated for the vibrational (null for H_2 and almost null for H_2S) and rotational parts of the chemical potentials of H_2S and H_2 . The translational parts were computed using the thermodynamical function in terms of the gas relative pressure [33]:

$$\mu_i^{\text{trans}} = -k_B T \ln \left(\frac{k_B T}{P_i} \left(\frac{2\pi m_i k_B T}{h} \right)^{3/2} \right) \quad (6)$$

P_i and m_i being the pressure and the mass of the particle i respectively

The ideal gas approximation is obviously inadequate for high partial pressures in gas phase. Flash calculations on the basis of the Soave Redlich Kwong equation of state (SKR EOS) with volume translation [35] give good estimates of the fugacities for $\text{H}_2 + \text{H}_2\text{S}$ mixtures as function of temperature and pressure. They can be readily extended to account for the presence of liquid and gaseous hydrocarbons in the reactor. For instance at 200 bar total pressure, a mixture of 0.9 mol fraction H_2 and 0.1 mol fraction H_2S corresponds to fugacities of 196 and 19.2 bar, 193.4 and 20.3 bar, 191.6 and 20.8 bar, for H_2 and H_2S at 473 K, 575 K and 675 K respectively. Eq. (6) as well as phase diagrams of Figs. 10 and 11 remains valid in terms of fugacities. We recommend using the SKR EOS for the evaluation of the corresponding real partial pressures.

3. Results

In this section, we start by presenting in Section 3.1 total energy and free-energy profiles along the reduction pathways of MoS_2 edges by dihydrogen, since the exploration of those pathways has been our strategy aiming at the determination of stable states

according to catalytic operating conditions, in a similar way as our previous works [4,34–37] and that of other authors [3,8,9]. Having thus identified the local minima in free-energy profiles, we construct in Section 3.2 surface phase diagrams allowing for the first time to identify the domains of prevalence of particular configurations at MoS_2 edges simultaneously as function of fugacities of H_2 , H_2S , and of temperature, and therefore in reference to relevant operating conditions for catalytic hydrotreating. Further, in Section 3.3, we check our theoretical predictions against the results of spectroscopic experiments available in literature. This is done by comparing observed vibrational frequencies for MoS_2 -based catalysts, prepared and analyzed in well defined conditions of temperature and fugacities of H_2 and H_2S , to our predicted frequencies assigned to surface groups' normal modes, as expected for those conditions according to our surface phase diagrams. Finally, in Section 3.4, we exhibit Brønsted–Evans–Polanyi relationships for the H_2 dissociative adsorption and H_2S associative desorption processes on MoS_2 edge surface, as outcomes of the free-energy profiles detailed in Section 3.1. From the latter, we therefore logically infer both the thermodynamic and kinetic consequences.

3.1. Free-energy profiles along reduction pathways of MoS_2 edges by dihydrogen

This sub-section is to some extent the continuation of our previous work [4], in which we have presented the free-energy profile along the partial reduction pathway starting from the Mo edge fully covered by sulfur dimers (M-edge 100%S) and leading to half-coverage by bridging S ad-atoms (M-edge 50%S). We therefore start with the reduction from M-edge 50%S to M-edge 37%S, which creates the first anionic vacancy in place of a bridging site. We verify then that the creation of the second anionic vacancy to give M-edge 25%S has a high free-energy penalty so that this state will not appear. We proceed similarly for the S-edge, starting again from the full coverage in sulfur (S-edge 100%S) and ending with the thermodynamically lesser favoured S-edge 37%S after creation of 5 vacancies.

3.1.1. M-edge (initial state 50%S)

3.1.1.1. Total energy profiles. The heterolytic dissociative adsorption of a H_2 molecule is found to be an exothermic process (−0.12 eV), as shown in Fig. 2 (S1 → S2). Moreover, the energy barrier is found to be close to 0.48 eV. A careful analysis of the critical parameters of the calculation leading to these values in comparison with the open literature is reported in Supplementary Material for sake of clarity. In comparison, the homolytic dissociative adsorption of H_2 on the M-edge with 100%S recently found by Dinter et al. [4] is less exothermic (−0.08 eV) but the activation energy higher (0.95 eV). In this latter case, the physisorbed precursor is slightly more bound (−0.20 eV).

Once the dissociative adsorption occurred on the edge, the diffusion of hydrogen ad-atoms is kinetically favoured compared with H_2 and H_2S associative desorption, the latter having to overcome the largest barrier. Thus, going through S2 and S3 states, diffusion leads to the most stable configuration (state S4_bis) of the reaction path, as shown in Fig. 2. This S4_bis state (see Fig. 3) is −1.09 eV more stable than the S1 state. It is reached by diffusion of H ad-atoms from the “trans” state S4, which is already −0.56 eV more stable than the S1 state (Sun et al. reported a stabilization by −0.37 eV for a closely similar configuration [10]). Notice that we find the “cis” S4 state destabilized by 0.19 eV with respect to “trans” S4, while the “cis” S4_bis state is −0.06 eV more stable than the “trans”. The pathways from S4 to S4_bis pass through TS3_bis/S3_bis/TS3_ter. The barrier to TS3_bis is 0.68 eV, a little lower than the barrier from S4 to S3 via TS3 (0.70 eV). The intermediate S3_bis between S4 and S4_bis is at −1.02 eV, almost as stable

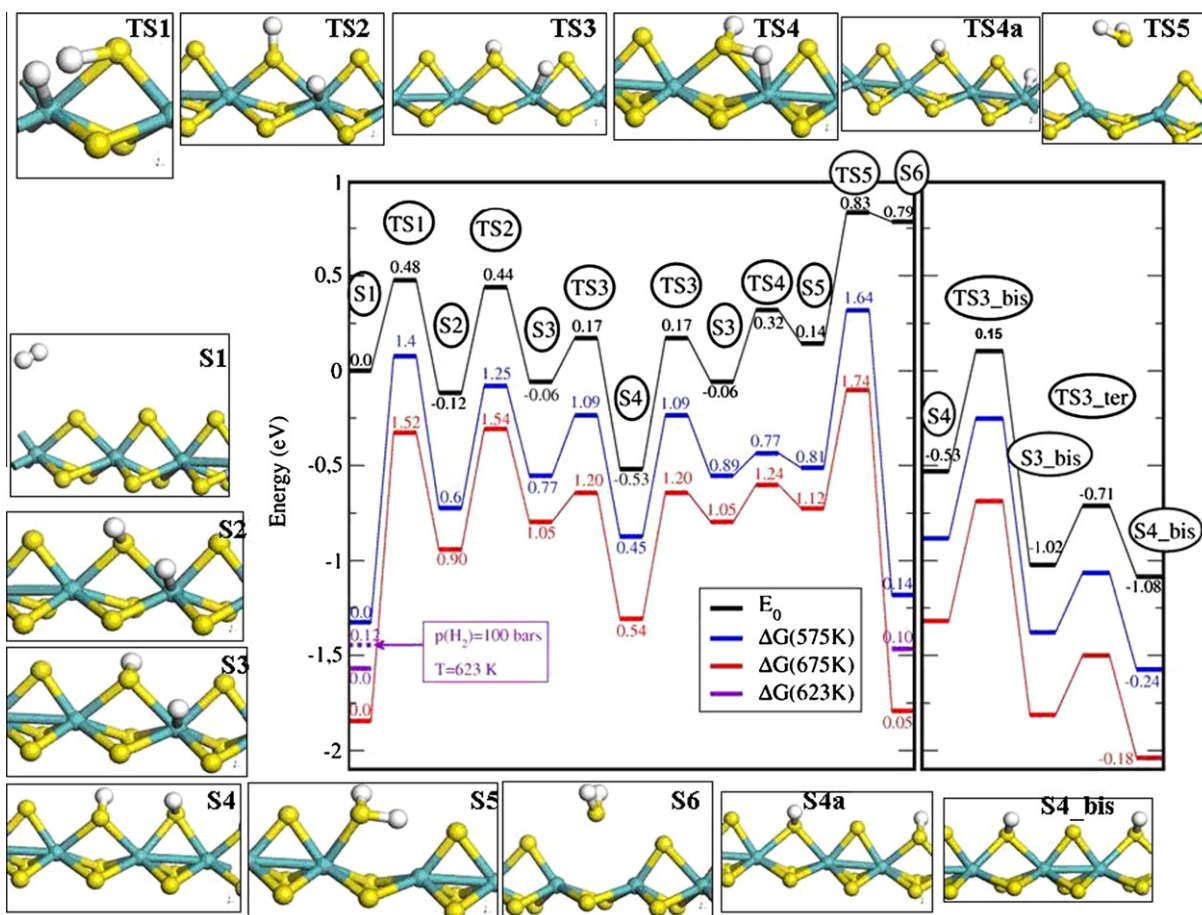


Fig. 2. Reaction pathway for the creation of one S vacancy on the M-edge 50%S. Blue line: Free energy at 575 K, $p_{H_2} = 10$ bar, $p_{H_2S} = 0.1$ bar ($\Delta\mu_S = -1.01$ eV). Red line: Free energy at 675 K, $p_{H_2} = 10$ bar, $p_{H_2S} = 0.1$ bar ($\Delta\mu_S = -1.13$ eV). Energies of the S1 state are taken as references for each reaction path. On the ordinates, axis is reported (purple dash) at 623 K the free energy of the S1 state at 100 bars and 10 bars of H_2 pressure and the S6 at 0.1 bar of H_2S pressure ($p_{H_2} = 10$ bar). Also the total energy, the free energy at 575 K and the free energy at 675 K of the S4_bis state (see Fig. 3) are reported.

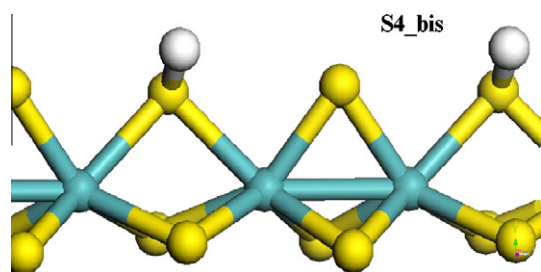


Fig. 3. Configuration of the most stable state on the M-edge 50%S (-1.09 eV), the S4_bis state, also called Me50S_SH_S_SH.

as S4_bis since the bridging S–H and the Mo–H are already separated by one bridging S. Further stabilization by -0.05 eV occurs with the diffusion of H along the next M–S bond, through transition state TS3_ter across a barrier of 0.31 eV. Here, we should emphasize that an even longer distance between hydrogens of sulfhydryl groups might furthermore stabilize the hydrogenated edge. Because of the repulsive interaction between sulfhydryl groups, diffusion is essential to reach the most stable state on the edge. In addition, increasing hydrogen coverage beyond 2 H per 4 S atoms is not energetically favourable as also found in [10] (see also Section 3.2).

It is clear from Fig. 2 that hydrogens are more stable when bonded to sulfur than when bonded to molybdenum. This is not

surprising as molybdenum atoms are already sixfold coordinated on the M-edge 50%S.

Starting from the S3 state, the desorption barrier is 0.89 eV (close to the value reported by Paul et al. for a similar process [9], 1.0 eV), but the overall barrier is much larger if one considers desorption from the S4 state, 1.36 eV ($0.83 - (-0.53)$), while the creation of a S vacancy is endothermic ($+1.32$ eV).

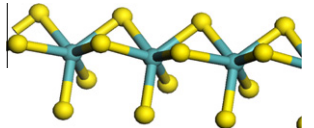
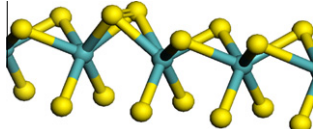
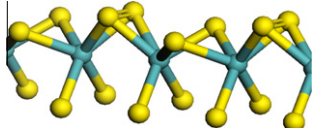
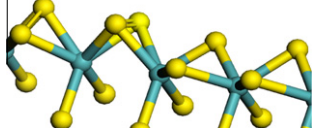
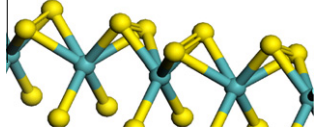
However, the overall reduction process starting with H_2 adsorption and ending up with H_2S desorption is much more favoured thermodynamically ($\Delta E = 0.79$ eV) and kinetically (barrier 0.83 eV) in comparison with Paul et al.'s results (1.31 eV and 1.47 eV respectively).

3.1.1.2. Thermodynamic corrections. In order to determine the stable configurations from a thermodynamic point of view, the thermodynamic contributions were included in Fig. 2 together with the total ground state DFT energy profile, giving estimates of the free-energy profiles at 575 K (blue¹ line) and 675 K (red line), under 10 bar of H_2 and 0.1 bar of H_2S representative of a range of relevant HDS operating conditions.

The thermodynamic corrections slightly change the reaction path although the tendency remains similar, i.e. the S4_bis state is the most stable along the reaction path involving H diffusion (S2–S5). Taking into account vibrational corrections decreases the

¹ For interpretation of color in all figures, the reader is referred to the web version of this article.

Table 1
Energy differences for different configurations of the S-edge 100%S, where the edge without dimer is taken as a reference for the energy.

Configurations	Energy (eV)		Models
	Our work	Reference*	
No “dimerized” S ₂ bridge	0.00	0.00	
One “dimerized” S ₂	-0.76		
2 “dimerized” S ₂ bridges alternately	-0.99	-1.16	
2 “dimerized” bridges side by side	-0.78		
4 “dimerized” S ₂ bridges	-0.67	-1.06	

* Corresponds to Ref. [38] where the cell contains 2 units of MoS₂ on the edge instead of 4 in our case.

activation energy for H₂S desorption to 1.19 eV and 1.20 eV at 575 and 675 K respectively compared to 1.36 eV for DFT energy alone. Moreover, the extra difference brought by vibrational energy and entropy could be as much as 0.19 eV (between S3 and TS4) along the H diffusion path. The most drastic difference (0.37 eV) is found for the adsorption–desorption process (between S1 and S3). Such corrections lie well beyond the accepted accuracy of DFT.

The S6 state is, at equilibrium, almost as stable as the S1 state, and its stability increases with temperature. This is interesting since this state involves an anion vacancy, which is an adsorption site for sulfided molecules like thiophenic homologs [36,37]. This point will be discussed further in Section 3.2.

3.1.2. S-edge

3.1.2.1. Total energy profiles.

3.1.2.1.1. initial state S-edge 100% S. A quick simulated annealing from 900 K down to 100 K afforded us to find a stable configuration for the S-edge, where a “dimerized” S₂ bridge appears, see Table 1 second row. This “dimerized” S₂ bridge appears to be more stable than the “separated” S₂ bridge. Several configurations have been computed with several “dimerized” S₂ bridges, all reported in Table 1: four “dimerized” S₂ bridges (in this configuration, the dimers bend on one side or the other alternately as mentioned by Bollinger et al. [17]), two S₂ dimers (with two possible configurations), and one S₂ dimer on the edge. The alternation of S₂ “dimerized” and “separated” S₂ bridges, further denoted as S1, is the most stable configuration (by -0.99 eV) as proposed by Hinnemann et al. [38], even more stable than four S₂ separated bridges. The change in vibrational normal modes between no “dimerized” bridge and one “dimerized” bridge on the edge reduces this energy difference by only at most 0.17 eV in free energy (at 675 K), whereas this reduction is almost null between one “dimerized” bridge and two “dimerized” bridges on the edge.

It appears that the proximity of “dimerized” S₂ bridges leads to a deformation of the structure, which becomes less stable: the energy raising by 0.21 eV when “dimerized” S₂ bridges are side by side instead of alternated. Besides we found, Fig. 4a) (S1–S2), that the activation energy for the separation of a “dimerized” S₂ bridge is 0.41 eV, but only 0.18 eV for the reverse process. The first dimerization on the edge is highly exothermic (-0.76 eV), but there is less stabilization associated with the creation of the second “dimerized” S₂ bridge (-0.23 eV).

Fig. 4a and b present two different pathways, diverging beyond S2 respectively with the homolytic dissociation of H₂ on the same bridging S₂ dimer, or adjacent dimers.

Fig. 4a represents the computed reaction pathway for the creation of a S vacancy on the S-edge 100%S. The first step (S1–S2 via TS1, over a 0.41 eV barrier) corresponds to the activated “opening” of the S=S bond of one dimer, where the dissociative adsorption of the H₂ molecule will further occur following a non-concerted mechanism. Then, the H₂ molecule is slightly physisorbed (-0.02 eV). The total activation energy for the H₂ homolytic dissociative adsorption is 0.86 eV, but it is lowered if the adsorption occurs directly on a separated bridge (0.65 eV). This is close to the one for the M-edge 50%S (0.48 eV), whereas the former is closer to the one for the M-edge 100%S (0.95 eV) [4].

Fig. 4b points out another pathway for the homolytic dissociative adsorption of H₂ on the S-edge 100%S (S2–S5 g). The activation energy (0.92 eV) is of the same order as the first one (0.86 eV), but the chemisorbed state directly accessible after the dissociative adsorption on two neighboring bridges is far more stable (-1.2 eV) than for the first reaction pathway on a single bridge (-0.48 eV). This value confirms earlier reported results [15,17,38], showing that H₂ adsorption on this edge is an exothermic process. A panel of configurations is proposed in Fig. 4b illustrating H diffusion along the S-edge 100%S. The most stable one

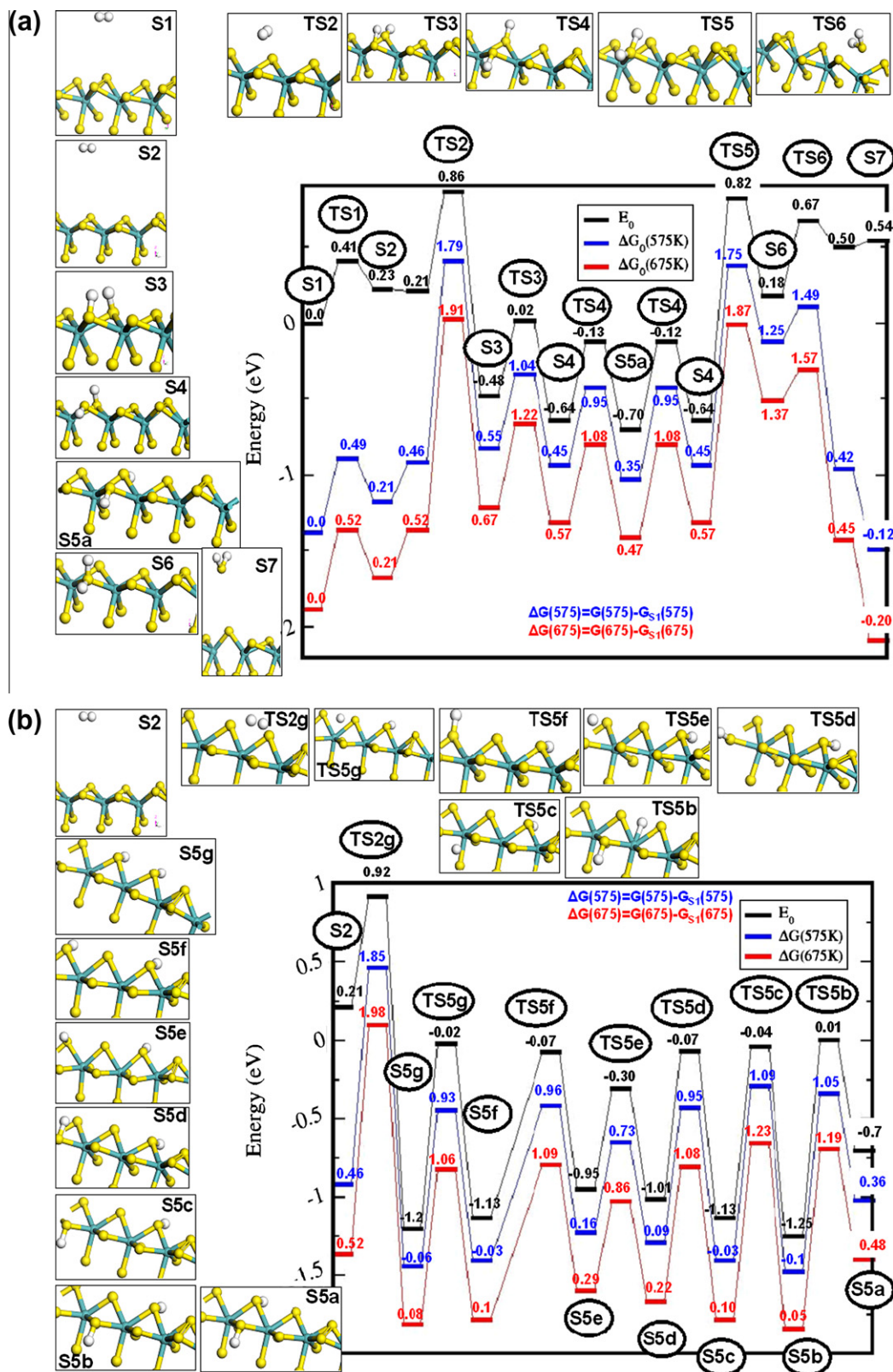


Fig. 4. (a) Reaction pathway for the H₂S desorption process on the S-edge 100%S, through H₂ adsorption on one bridge. The first step is the separation of the 'dimerized' Sulfur in the bridge. Blue line: Free energy at 575 K, pH₂ = 10 bar, p_{H₂S} = 0.1 bar. Red line: Free energy at 675 K, pH₂ = 10 bar, p_{H₂S} = 0.1 bar. Energies of the S1 state are taken as references for each reaction path. (b) H₂ adsorption on two neighboring bridges and diffusion along the S-edge 100%S (S2 and S5a states are equivalent to those on figure a. Blue line: Free energy at 575 K, pH₂ = 10 bar, p_{H₂S} = 0.1 bar. Red line: Free energy at 675 K, pH₂ = 10 bar, p_{H₂S} = 0.1 bar. Energies of the S1 state (in figure a) are taken as references for each reaction path. Note that the most stable state at 0 K is S5b, while at 675 K (red path) it becomes S7.

Table 2

Bader analysis of the electronic charge borne by Mo and S atoms contained in the MoS₂ catalyst sheets. Since the pseudopotential we used contained 6 valence electrons for each atom, the net charge on each atom is deduced from the electron valence charge of the Bader analysis [28,29].

	Bader analysis of the valence charge	Net Charge on atoms
<i>S-edge 100%S</i>		
S at the edge		
Dimerized bridge	6.40 e	-0.40 e
Separated bridge	6.78 e	-0.78 e
S in the inert plane	6.85 e	-0.85 e
Mo near the edge	4.21 e	+1.79 e
Mo in the inert plane	4.30 e	+1.70 e
<i>S-edge 50%S</i>		
S at the edge		
S in the inert plane	6.96 e	-0.96 e
Mo near the edge	6.85 e	-0.85 e
Mo in the inert plane	4.21 e	+1.79 e
Mo in the inert plane	4.30 e	+1.70 e

(S5b state) occurs when H atoms are bonded on neighboring S₂ bridges alternatively on one side and on the other (-1.25 eV/H₂ where the reference is taken as the S1 state). It is of importance to notice that on this edge, for 100% sulfur coverage, hydrogens are not stable on molybdenum atoms, which is not so surprising since Mo atoms are already sixfold coordinated. Simultaneously, the electronic charge is localized on sulfur as exhibited in Table 2.

While one hydrogen bonded on a S₂ bridge will decrease its basic character, it can be noticed that the (qualitative) contrast in the acido-basic characters of the bridges in the initial and final configurations gives a trend in the activation energy: when this contrast is strong, e.g. SHSH bridge and S₂ bridge (S5a–5b: E_a = 0.71 eV) or SH bridge and S bridge (S5e–S5d: E_a = 0.65 eV), the reaction is favored. When the contrast is weaker, the reaction is less favored, e.g. SSH bridge and S₂ bridge (S5g to S5f and reversely: E_a = 1.18 and 1.11 eV) or SSH bridge and SSH bridge (S5b to S5a: E_a = 1.26 eV). Those diffusion processes are faster than H₂ or H₂S associative desorptions, which have almost the same reaction barriers (see Fig. 4a) respectively S3 → S2, 1.34 eV, and S4 → S7, 1.46 eV).

The physisorbed molecular state following S2, and precursor to the homolytically dissociated S3 state (see Fig. 4a), contains a fraction of the translational and rotational contributions to the free energy prevailing in gas phase. In order to take into account the part of the free energy remaining in this state, we apply a fraction of order 0.5, as previously proposed by Dinter et al. for physisorbed H₂ and H₂S molecules [4,32] (Notice that no physisorbed states of H₂ or H₂S were found on M-edge 50%S, see Fig. 2.)

Including the thermodynamics corrections at 575 and 675 K with p_{H₂} = 10 bar and p_{H₂S} = 0.1 bar, the S-edge 87%S (S7) is more stable than the hydrogenated S-edge 100%S (S3–S5a–g) and the non-hydrogenated S-edge 100%S (S1 and S2). Raising the temperature increases the stability of the desorbed state, which is not surprising, since the entropy of translation–rotation of H₂S increases with temperature.

Adsorbing one more H₂ molecule on the hydrogenated S-edge 100%S leads to a state called S-edge 100%S + 50%H (in which half of the terminal sulfur atoms are bonded with one hydrogen atom, as shown on Fig. 5b). This state is stabilized by -1.3 eV per adsorbed H₂ molecule, therefore more stable than S5b. In the same conditions as mentioned above, the free energy of adsorption of 2 H₂ molecules is -0.24 eV at 623 K with a 10 bars H₂ pressure (-0.36 eV at 575 K and -0.12 eV at 675 K). Then, with 4 adsorbed H₂ molecules per unit-cell, the fully H-saturated S-edge 100%S

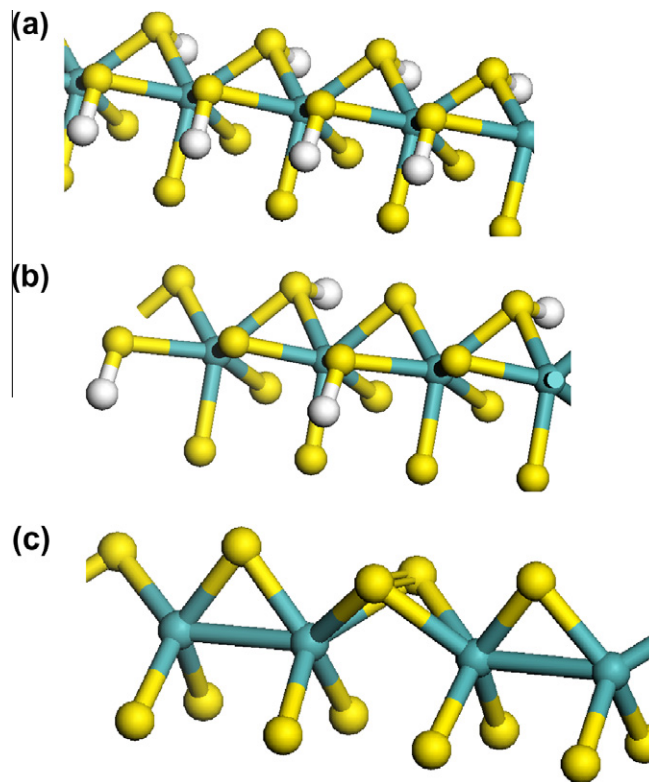


Fig. 5. (a) S-edge 100%S + 100%H and (b) S-edge 100%S + 50%H respectively 1.3 eV and 2.6 eV lower in energy than S1 state with H₂ in gas phase, i.e. -0.325 eV and -1.3 eV adsorption energy per H₂ molecule, (c) configuration of the S-edge 62%S involved in the phase diagram of Fig. 11.

100%H has been considered (Fig. 5a), but due to the repulsive interactions between neighboring hydrogens, this state is destabilized by almost 1 eV per adsorbed H₂ with respect to the S-edge 100%S + 50%H. The latter will therefore dominate at relevant HDS conditions as will be discussed further in Section 3.2, and as shown on Fig. 12a).

It is worth mentioning that the vibrational contribution to free-energy differences between chemisorbed states can reach 0.21 eV (between TS5g and S5b), and as much as 0.57 eV between desorbed and chemisorbed state (between S2 and S5b). It is then clear that omitting this difference would lead to misleading activation free-energy barriers and phase diagrams.

3.1.2.1.2. initial state S-edge 87%S. This state is the continuation of the S-edge 100%S after the desorption of one H₂S molecule and relaxation of the edge, so seven sulfur atoms remain on the edge, that is 87.5% sulfur coverage and two “dimerized” S₂ bridges (state S10 on Fig. 6).

We now focus on the effect of one S bridge as first neighbor of the S₂ bridge where a H₂S desorption occurs. The left part of Fig. 6 represents the diffusion of H from a S₂ bridge to a S bridge site (S11–S12) on the S-edge 87%S. S12 is the most stable state with H ad-atoms on the S-edge 87%S. We assume that the barrier to H diffusion inside the S bridge (S12–S13) is close to that prevailing for the similar process on the S-edge 100%S (S5f–S5c). Finally, the H₂S associative desorption process is carried out between one S bridge site and the vicinal S₂ bridge site (S13–S15).

The S10_{bis} configuration (not reported here) is similar to S11 without hydrogens. Its energy level is 0.21 eV higher than the S10 configuration, from which it differs by the “opening” of one S₂ dimer. This is almost the same difference as on the S-edge 100%S between S1 (alternation of “dimerized” bridge and “separated” bridge) and S2 (only one “dimerized” bridge) also previously

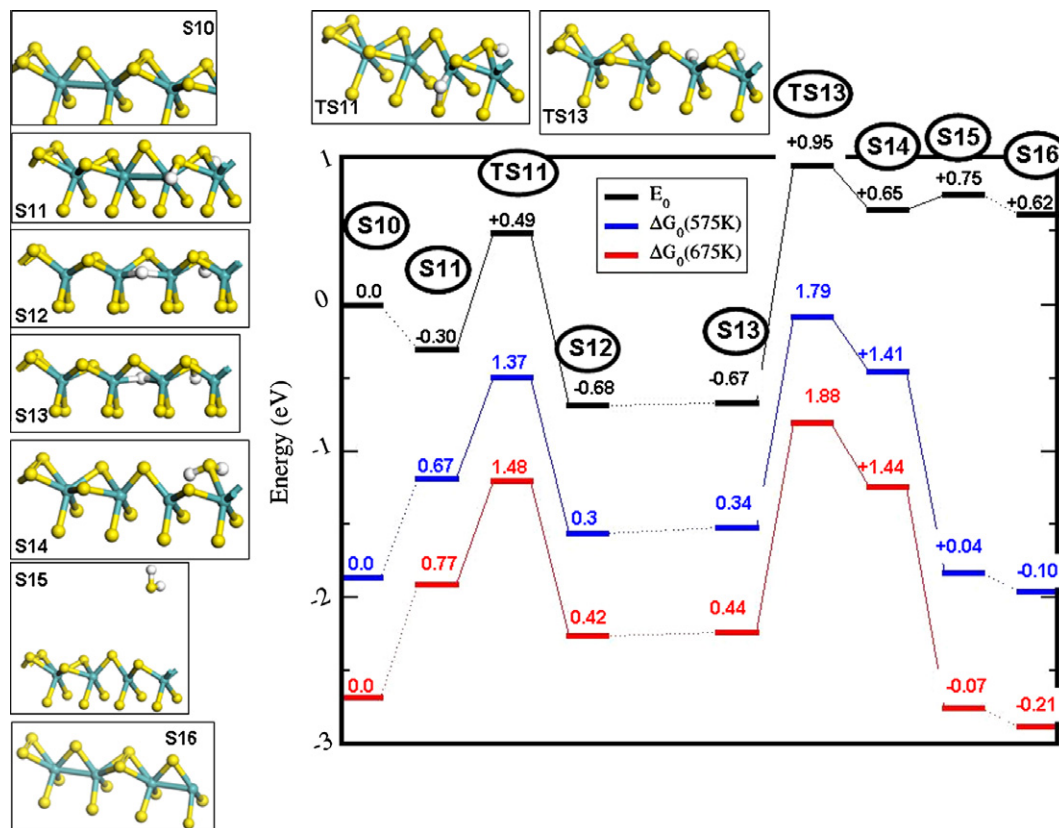


Fig. 6. Reaction path for H₂S desorption from the 87%S-edge. Blue line: Free energy at 575 K, p_{H₂} = 10 bar, p_{H₂S} = 0.1 bar. Red line: Free energy at 675 K, p_{H₂} = 10 bar, p_{H₂S} = 0.1 bar. Each reference energy is the energy of the S10 state for each reaction path. Note that the S15 configuration is less favorable by $\Delta G(T) = -0.13$ eV (the dependence in temperature in the range of interest is less than 0.01 eV) than S16, where 'dimerized' S₂ bridge alternate with S bridges on the edge. (For simplification, H₂ molecule in inset S10 and H₂S molecule in insets S16 have been omitted.)

presented in Table 1. It seems that whatever the configuration without H, "dimerizing" every two S₂ bridges stabilizes the configurations by 0.2 eV.

On the 87%S-edge, hydrogen is more stable on the bridge site between molybdenum atoms supporting the bridging sulfur atom (S12 and S13) than bonded to a sulfur atom of the vicinal S₂ bridge, or of the S bridge itself (by about +1 eV from S12, not represented in Fig. 6). One should notice that as for S-edge 100%S, hydrogen is not stable on a single molybdenum atom (which is sixfold coordinated).

With thermodynamic corrections included along the reaction path (blue and red lines in Fig. 6), it appears that the 75%S configuration (S15) is slightly more stable than S10 at 675 K, but this stabilization decreases with decreasing temperature.

Finally, the configuration reached after H₂S desorption is not the most stable of the S-edge 75%S. Indeed, the most stable configuration contains alternating "dimerized" S₂ and S bridges (S16), which can be reached through S diffusion on the edge. This latter configuration is slightly more stable ($\Delta G(T) = -0.13$ eV almost independently of temperature) than the former one, and slightly more stable than the S-edge 87%S at 575 K and 675 K.

It is important to notice that the difference in free energy due to the changes in normal vibrational modes can reach 0.32 eV between the chemisorbed states (S14–S13) and 0.39 eV between chemisorbed and desorbed state (S13–S15).

The state S16 is S-edge 75%S. In what follows, we will assume, in view of the local similarities of starting configurations (neighboring S₂ dimer and bridging S), that the reduction pathways transforming the two remaining S₂ dimers into S bridges, that is from S-edge 75% to S-edge 62%S (Se62S), then from S-edge 62%S

to S-edge 50%S (S21) will be similar to that shown in Fig. 6 to go from S10 to S16. The latter has been therefore detailed because of its prototypical character. Although we have computed the conformations and free energies of the S-edges 75% and 62%, which are included in Section 3.2 below, the present assumption will have to be verified when precise barriers and free-energy levels of the corresponding intermediates will be needed.

3.1.2.1.3. initial state S-edge 50% S. Fig. 7 presents two reaction paths going from H₂ homolytic dissociative adsorption (S21–S22) on S-edge 50%S to H₂S associative desorption (S23–S30), and H₂S chemisorption (S30–S24) to H₂ associative desorption (S25–S21). Notice that the reverse of the latter pathway (S21–S25) corresponds to heterolytic dissociation of H₂ which is then shown, as discussed below, to be preferred over the homolytic pathway on this particular edge. No transition state was found for H₂S desorption, so TS30 and S30 have been displayed with the same energy in the total energy profile.

The sequence of elementary steps for H₂ dissociative adsorption is similar to those presented by Paul and Payen [9] and Sun and Nelson [10]. The H₂ molecule enters the physisorbed S26 state after a 0.2 eV barrier has been passed at the TS26 transition state. Similar to the proposals by Paul and Sun (0.09 eV and 0.23 eV respectively), this step is slightly endothermic by 0.16 eV. Then, the activation barrier for this heterolytic dissociative adsorption is 0.62 eV, pretty close to the value of 0.6 proposed by Paul, and lower than the value of 0.99 eV proposed by Sun. This step is exothermic by -0.19 eV in our case, to be compared to -0.23 eV presented by Paul and 0.02 eV by Sun. The other way, homolytic dissociative adsorption, has not been computed by Paul and Sun, but is unlikely to occur, as there is no physisorbed state, and the activation energy

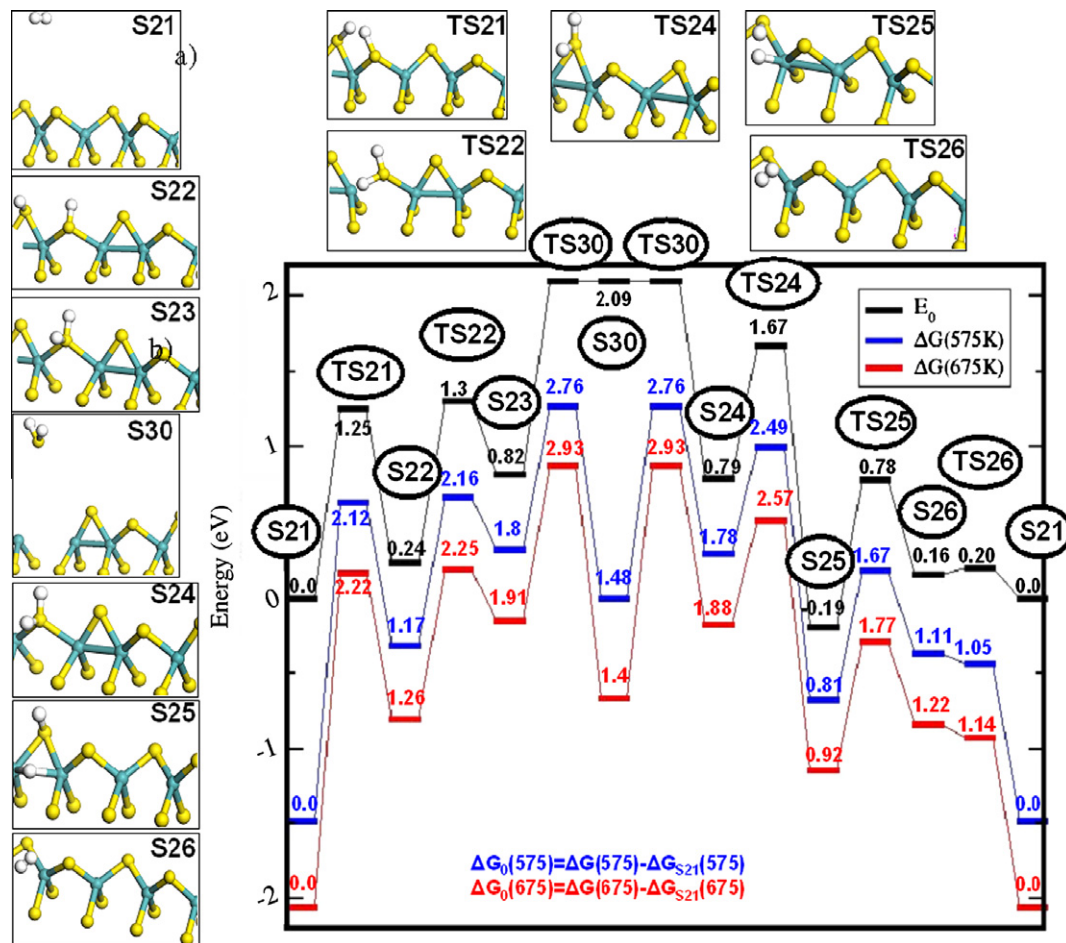


Fig. 7. Reaction path on the S-edge 50%S for the H₂ homolytic dissociative adsorption on two neighboring S bridges (S21–S22), then H₂S desorption (S23–S30), followed by H₂S adsorption (S30–S24), eventually H₂ heterolytic associative desorption via a SH-H group (S25) on the 50%S-edge (the reverse reaction path S21–S25 corresponds to a heterolytic dissociative adsorption of H₂ on this edge, which turns out to be easier). Blue line: Free energy at 575 K, p(H₂) = 10 bar, p(H₂S) = 0.1 bar. Red line: Free energy at 675 K, p(H₂) = 10 bar, p(H₂S) = 0.1 bar. Energies of the S21 state are taken as references for each reaction path.

is relatively high compared to the previous one (1.25 eV). The adsorbed state subsequent to this step (S22) is higher in energy by 0.24 eV than S21; therefore, homolytic dissociative adsorption is now endothermic.

The sulfur bond energy on the S-edge 50%S is huge (2.09 eV) in comparison with the other S-edges. The sulfur bond energy thus increases with decreasing sulfur coverage as expected by Raybaud et al. [34].

Fig. 8 presents the reaction path of H diffusion along the S-edge 50%S. H is now more favoured on the bridge site between adjacent molybdenum atoms than bonded to the sulfur atoms (S29a and S29b in comparison with S22). This seems to confirm the basic character of the bridge site lying between 2 molybdenum atoms.

The free-energy differences due to changes in normal vibration modes are still important on this edge. Between chemisorbed states, the difference can reach 0.31 eV (S29b to TS24) and until 0.47 eV between chemisorbed and desorbed states (S29b–S21).

3.2. Surface phase diagrams revisited

It is convenient to express the H₂ and H₂S pressures (or rather fugacities) in terms of chemical potential. Thus:

$$\Delta\mu_{\text{H}} = \mu_{\text{H}} - \frac{1}{2}E_{\text{H}_2} \quad \text{and} \quad \Delta\mu_{\text{S}} = \mu_{\text{S}} - \mu_{\text{S}}(\text{bulk}) \quad (7)$$

with μ_{H} and μ_{S} computed according to the method detailed in Section 2.2, and E_{H_2} and $\mu_{\text{S}}(\text{bulk})$ respectively the total energy of H₂

computed in DFT and the total energy of sulfur in alpha crystalline phase.

In what follows, “relevant HDS conditions” are defined in terms of temperature interval (573–700 K), partial pressure of H₂ p(H₂) (1–200 bar), and ratio of partial pressures p(H₂S)/p(H₂) (10⁻⁴–10⁻¹). Indeed, industrial hydrotreating units are operated at p(H₂) ranging from a few bar (HDS of naphas as pretreatment of reforming feedstocks) to almost 200 bar (hydroconversion of vacuum residua), and temperature ranging from about 573 K to about 700 K. The ratio p(H₂S)/p(H₂) lies most often between 0.01 and 0.05. Besides experiment performed on model molecules at the laboratory scale, or spectroscopic experiments may include p(H₂) slightly over one atmosphere (taking into account pressure drops across small fixed beds of catalysts), and in general p(H₂S) might be very low; however, we assume they will stay above the limit of stability of MoS₂ with respect of Mo metal. Finally, our definition of “relevant HDS conditions” tries to encompass all these situations corresponding to a possible experiment involving a MoS₂-based catalyst.

In Fig. 9 are plotted the grand potentials of several M-edge configurations relative to the grand potential of the S1 state, against the chemical potential of sulfur relative to its alpha crystalline phase, $\Delta\mu_{\text{S}} = \mu_{\text{S}} - E_{\text{S}}^{\text{bulk}}$. Here, these grand potentials correspond to the free enthalpies of reactions connecting S1 to the other states, $\Delta G(T, p(\text{H}_2), p(\text{H}_2\text{S}))$, plotted for $T = 623$ K and $p(\text{H}_2) = 10$ bars. A large set of configurations was simulated for each type of edge (S coverages and H coverages), but for clarity only the most stable

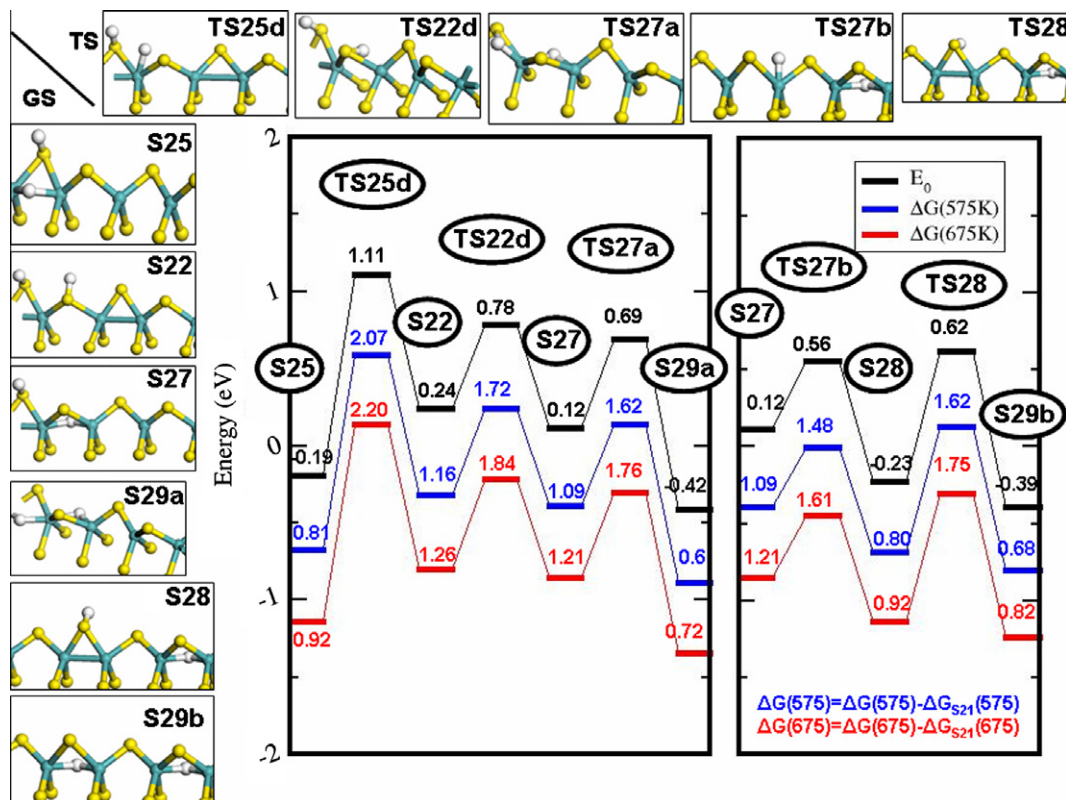


Fig. 8. Reaction path for the diffusion of H on the 50%S-edge. Blue line: Free energy at 575 K, $p_{H_2} = 10$ bar, $p_{H_2S} = 0.1$ bar. Red line: Free energy at 675 K, $p_{H_2} = 10$ bar, $p_{H_2S} = 0.1$ bar. Energies of the S21 state (see Fig. 7) are taken as references for each reaction path.

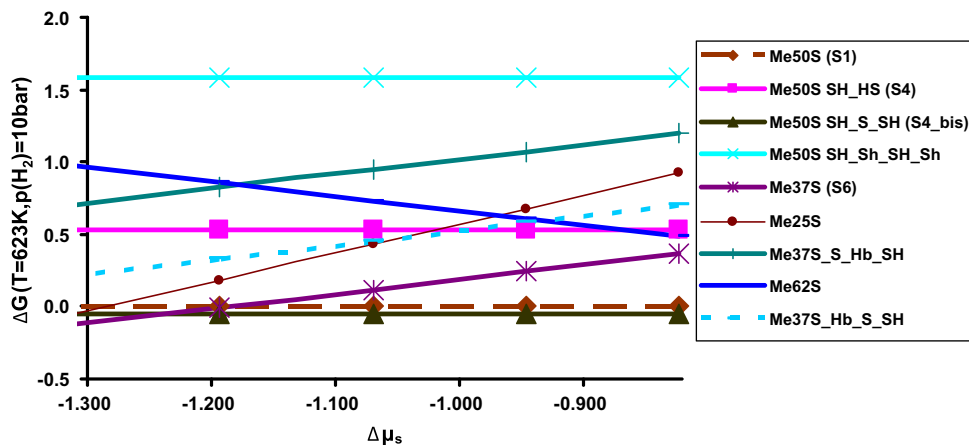


Fig. 9. Gibbs energy (at $T = 623$ K and $P(H_2) = 10$ bars) of several states on the M-edge 50%S according to the non-hydrogenated M-edge 50%S (Me50S) in terms of the Sulfur chemical potential. The Me50S_SH_S_SH state corresponds to the S4_bis state, and the state Me50S_SH_HS corresponds to the S4 state.

for each type of edge are reported. This figure displays the range of stability of non-hydrogenated M-edge 50%S states, and the M-edge 50%S + 50%H with 2 H on the surface (S4_bis state, see Fig. 3).

One can notice that at low chemical potential of sulfur, below -1.22 eV (i.e. H_2S pressure < 560 Pa), the M-edge 37%S (S6) becomes the most stable. However, its hydrogenated counterpart, Me37S_Hb_S_SH, is not stable. This is partly due to the loss of entropy in the chemisorbed state of H: the vibration free energy is higher for the hydrogenated edge state than for the other one; however, it is still compensated by the loss in translation and rotation entropies. This means that the probability that hydrogen remains adsorbed at the sulfur-vacancy site is very small, so that this site shall remain available for adsorption of other reactants.

The phase diagram at 623 K shown in Fig. 11 reveals the stability of three configurations in relevant HDS conditions, the S1 state, the S4_bis state, and the S6 state, consistently with Fig. 9. At very high $p(H_2S)/p(H_2)$ ratio ($\Delta\mu_s > -0.33$ eV), the M-edge 62%S becomes the more stable, but this is far out of relevant HDS conditions. The stability of a sulfur-vacancy on the M-edge (S6) is consistent with previous DFT calculations [39,40], showing that a coordinately unsaturated Mo site (Mo-CUS) can be stabilized in relevant HDS conditions. This corresponds to a S coverage on the surface around 37%. Lower S coverages explored so far, M-edge 25%S in the present work, or M-edge 33%S [34], are not stabilized, which means that a good estimate of S coverage at the edge is close to 37%S corresponding to 50% Mo-CUS.

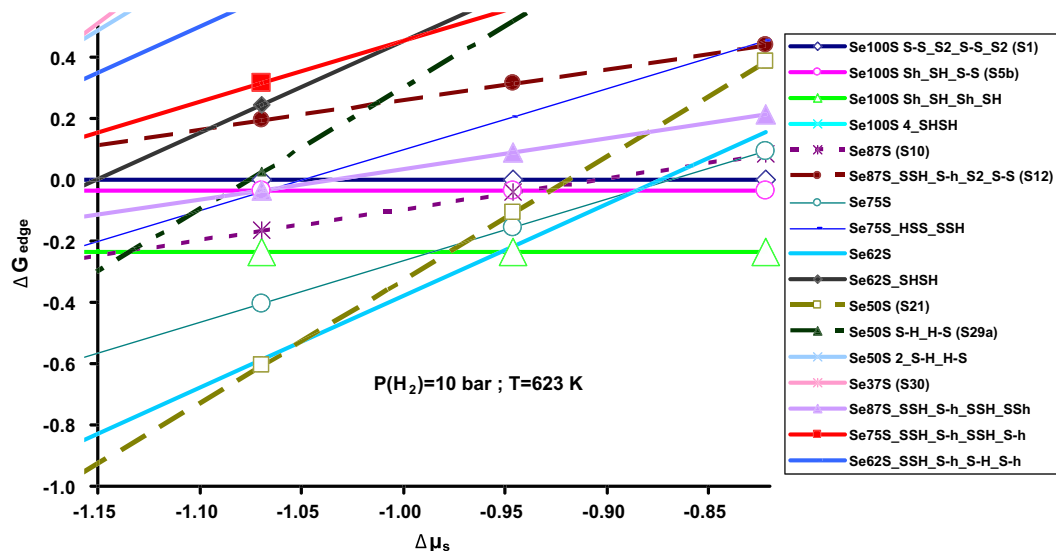


Fig. 10. Free energy of the S-edge for different configurations according to the Sulfur chemical potential at $T = 623$ K and 10 bar of H_2 pressure.

At 623 K, H is thermodynamically stable on the M-edge above 5.3 bar of H_2 pressure, and the configuration with the anion vacancy (S6) is stable for a ratio $p(H_2S)/p(H_2) < 10^{-3}$. A decrease in temperature (473 K in Fig. 13a) extends the stability domain of the S4_bis state toward lower values of H_2 pressure (now stable above $p(H_2) = 0.2$ bar) and lessens the domain of the S6 state (now stable below $p(H_2S)/p(H_2) \approx 2.10^{-5}$).

The coexistence of the S4_bis and S6 configurations is expected to favor HDS reactions, since the S6 state presents an adsorption site for sulfided molecules, which could then undergo hydrogenation and hydrogenolysis thanks to available H ad-atoms diffusing from the S4_bis state.

The two symbols in Fig. 11 represent the following conditions: temperature = 623 K and $p(H_2S) = 0.1$ bar, and $p(H_2) = 10$ bars for the crossed full square, and $p(H_2) = 100$ bars for the full triangle. These conditions correspond to the purple dashes for the S1 and the S6 states in the energy profile, Fig. 2. The two figures are consistent since the “M-edge” 37%S (S6 state) becomes more stable than the M-edge 50%S (S1 state) when increasing the H_2 pressure above about 100 bars.

In Fig. 10 are plotted the Gibbs energies of all the most stable computed configurations for each kind of S-edge (S coverage, H coverage) against the sulfur chemical potential $\Delta\mu_s$, at 623 K and $p(H_2) = 10$ bar. We observe that S-edge 100%S + 50%H with 4 hydrogens on the edge (Se100S Sh_SH_sh_SH) is the most stable for high $\Delta\mu_s$ (high H_2S pressure), whereas S-edge 50%S (Se50S or S21) is the most stable for low $\Delta\mu_s$ (low H_2S pressure), and S-edge 62%S (Se62S, see Fig. 5c) is the most stable in between.

Fig. 12a depicts a phase diagram of the S-edge at 623 K. In relevant HDS conditions ($p(H_2)$ between 1 bar and 200 bar, and $p(H_2S)/p(H_2) < 0.1$), that is inside the domain delimited by dashed lines, all the S-edge configurations represented in the diagram may be reached except 100%S. Changes in temperature, H_2 pressure, or H_2S pressure, will change the stable phase, and these changes will change the sulfur coverage on the edge. Each S bridge is an anion vacancy site potentially able to accept another sulfur to form a S_2 bridge. S-edge coverage changes from one stable state to another upon a change of reaction conditions.

The phase diagram in Fig. 12a exhibits a stability domain for the S-edge 100%S until a maximal H_2 pressure of 0.8 bar ($\Delta\mu_H = -0.41$ eV) and a minimal $p(H_2S)/p(H_2)$ ratio of 0.4 ($\Delta\mu_S = -0.88$ eV). Then, if the H_2 pressure is further increased, H chemisorption becomes strongly exothermic, and for dissociative

adsorption of up to two H_2 molecules on one S-edge, the more H chemisorbed on the edge, the more stable the edge. Then, at a constant H_2 pressure, decreasing the H_2S pressure favors the H_2S desorption from the S-edge 100%S 50%H, to S-edge 62%S or even S-edge 50%S. The state S-edge 62%S is stable down to $p(H_2S)/p(H_2) = 0.02$ ($\Delta\mu_S = -1.03$ eV). All these states have domains of stability intersecting the domain of relevant HDS conditions.

The crossed square dots in Figs. 11 and 12 represent a particular HDS condition, i.e. 623 K, $p(H_2) = 10$ bar and $p(H_2S)/p(H_2) = 0.01$. This particular HDS environment stabilizes the S-edge 50%S and the M-edge 50%S + 50%H (see Fig. 11). In these conditions, hydrogen is stable solely on the M-edge.

In Fig. 13 are reported the phase diagrams for the M-edge and S-edge in HDS conditions at 473 and 573 K. The comparison with phase diagrams at 623 K of Figs. 11a and b, and 12 points out the monotonic behavior of the evolution of the stability domains for the different surface phases with temperature.

On the M-edge, an increase in temperature tends to reduce the stability of chemisorbed hydrogen in relevant HDS conditions. The stability of a sulfur-vacancy on the edge (S6) increases with temperature, and at 623 K this domain is extended until a maximal $p(H_2S)/p(H_2)$ ratio of 10^{-3} , and a H_2 pressure up to 40 bars at $p(H_2S)/p(H_2) 10^{-4}$.

On the S-edge, at the lower temperature (473 K), the 100%S + 50%H edge holds on a large domain of pressure, in the relevant HDS conditions (inside the area delimited by dashed lines). It remains stable even for a H_2 pressure lower than 0.1 bar. The rest of the domain of relevant HDS conditions is filled by the S-edge 50%S. Notice that the S-edge 100%S is stabilized by the presence of hydrogen on the edge. When increasing the temperature, this domain and the 62%S domain are pushed toward larger values of the $p(H_2S)/p(H_2)$ ratio. This evolution (Figs. 12a and 13b and d) is observed through the change of the different domains containing the crossed square dot ($p(H_2) = 10$ bar, $p(H_2S) = 0.1$ bar).

3.3. Normal modes of vibration for edge SH and MoH groups

As indicated above, the vibration frequencies of normal modes were computed in order to calculate the phase diagrams. As a consistency test, it is worth comparing predicted and experimental frequencies, since the latter should reflect the presence of species at the conditions of preparation of the studied samples for spectroscopic experiments.

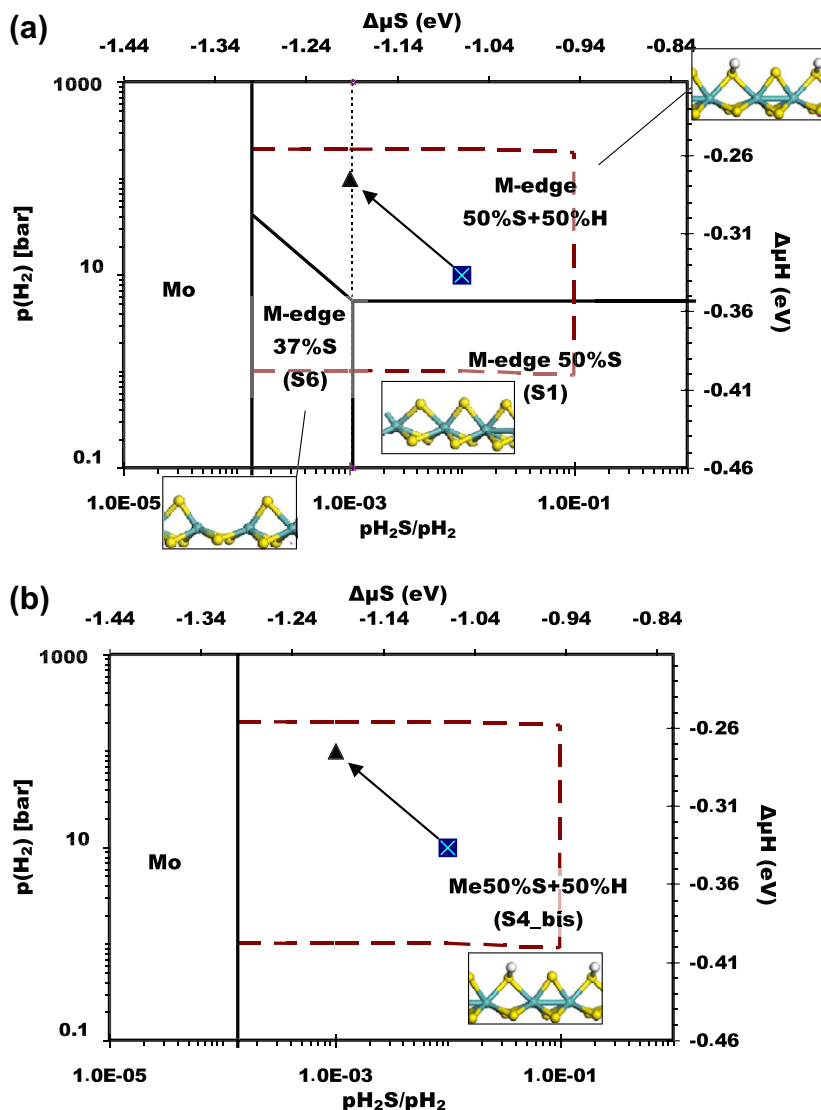


Fig. 11. (a) Phase diagram at 623 K, on the M-edge 50% S, in terms of the H₂ relevant HDS conditions (bounded by the brown dashed lines, total pressure between 1 and 200 bar and ratio $< 10^{-1}$), corresponding to S1, S6, S4_bis state (see Figs. 2 and 3). The dashed narrow black line represent the continuation of the limit between the S1 state and the S6 state. The crossed square dot represents the following conditions: $p(\text{H}_2) = 10$ bars, $p(\text{H}_2\text{S}) = 0.1$ bar and temperature = 623 K as indicated by Bollinger et al. [17], [18]. The triangle dot represents the following conditions: $p(\text{H}_2) = 100$ bars, $p(\text{H}_2\text{S}) = 0.1$ bar and Temperature = 623 K. (b) Same as (a) but without including thermal and entropic corrections on surface states energies.

This comparison is presented in Table 3. The 529 cm^{-1} vibration frequency of the S–S dimer on the S-edge has been brought out by Raman spectroscopy by Polz et al. [41] in experimental conditions for which we predict the coexistence of S-edge 62%S and M-edge 50%S (S1) (573 K, $P(\text{H}_2)$ 350–400 mbar, $\Delta\mu_S = -0.89$ eV). This frequency is in close agreement with our calculation (536 cm^{-1}) for the dimer belonging to the S-edge 100%S 25%H (S5 g). Besides its presence on the S-edge 100%S, this S–S dimer also exists on the S-edge 62%, and its computed vibration frequency now corresponds to 548 cm^{-1} , also very close to the experimental one. The agreement between the theoretical and the experimental frequencies for these particular conditions (575 K, $\Delta\mu_S = -0.89$ eV, $p\text{H}_2 = 300$ mbar) is therefore consistent with the predicted stability of the S-edge 62%S in our phase diagram.

Our computation of the normal modes for several configurations shows that, consistent with the experimental data [42] and corroborated by other theoretical works [43,16], the S–H bond stretching vibration frequencies are around 2500 cm^{-1} both on S-edge and on M-edge. Inelastic neutron scattering (INS) spectroscopy undertaken by Sundberg et al. [42] enables to assess indirectly vibration frequencies of edges at 473 K and under 1 bar, 20 bar or 50 bar of H₂ pressure. After pre-sulfidation at 573 K with a $p\text{H}_2\text{S}/p\text{H}_2$ ratio of 10% and 2 h in the conditions mentioned previously, first the temperature was decreased to 273 K, then the chamber was evacuated for one hour to remove H₂ from the gas phase, and finally the sample was cooled down to 60 K before beginning the spectroscopy measurements. The bending vibration frequency of S–H bonds reported at 650 cm^{-1} with INS spectroscopy corresponds in our table to the frequencies between 490 and 690 cm^{-1} . The theoretical bending frequencies of the S–H bond on the S-edge 100%S + 50%H ($676\text{--}658\text{ cm}^{-1}$) is in relatively good agreement with the experimental data since we find that the thermodynamically stable domain of the S-edge 100%S + 50%H extends toward the lower values of the ratio $p\text{H}_2\text{S}/p\text{H}_2$ with the decrease in temperature. On the M-edge, the frequencies of the bending vibration of the S–H bond found on the most stable hydrogenated edge (S4_bis: $644\text{--}496\text{ cm}^{-1}$) are somewhat lower than the typical experimental frequency. This discrepancy could

copy undertaken by Sundberg et al. [42] enables to assess indirectly vibration frequencies of edges at 473 K and under 1 bar, 20 bar or 50 bar of H₂ pressure. After pre-sulfidation at 573 K with a $p\text{H}_2\text{S}/p\text{H}_2$ ratio of 10% and 2 h in the conditions mentioned previously, first the temperature was decreased to 273 K, then the chamber was evacuated for one hour to remove H₂ from the gas phase, and finally the sample was cooled down to 60 K before beginning the spectroscopy measurements. The bending vibration frequency of S–H bonds reported at 650 cm^{-1} with INS spectroscopy corresponds in our table to the frequencies between 490 and 690 cm^{-1} . The theoretical bending frequencies of the S–H bond on the S-edge 100%S + 50%H ($676\text{--}658\text{ cm}^{-1}$) is in relatively good agreement with the experimental data since we find that the thermodynamically stable domain of the S-edge 100%S + 50%H extends toward the lower values of the ratio $p\text{H}_2\text{S}/p\text{H}_2$ with the decrease in temperature. On the M-edge, the frequencies of the bending vibration of the S–H bond found on the most stable hydrogenated edge (S4_bis: $644\text{--}496\text{ cm}^{-1}$) are somewhat lower than the typical experimental frequency. This discrepancy could

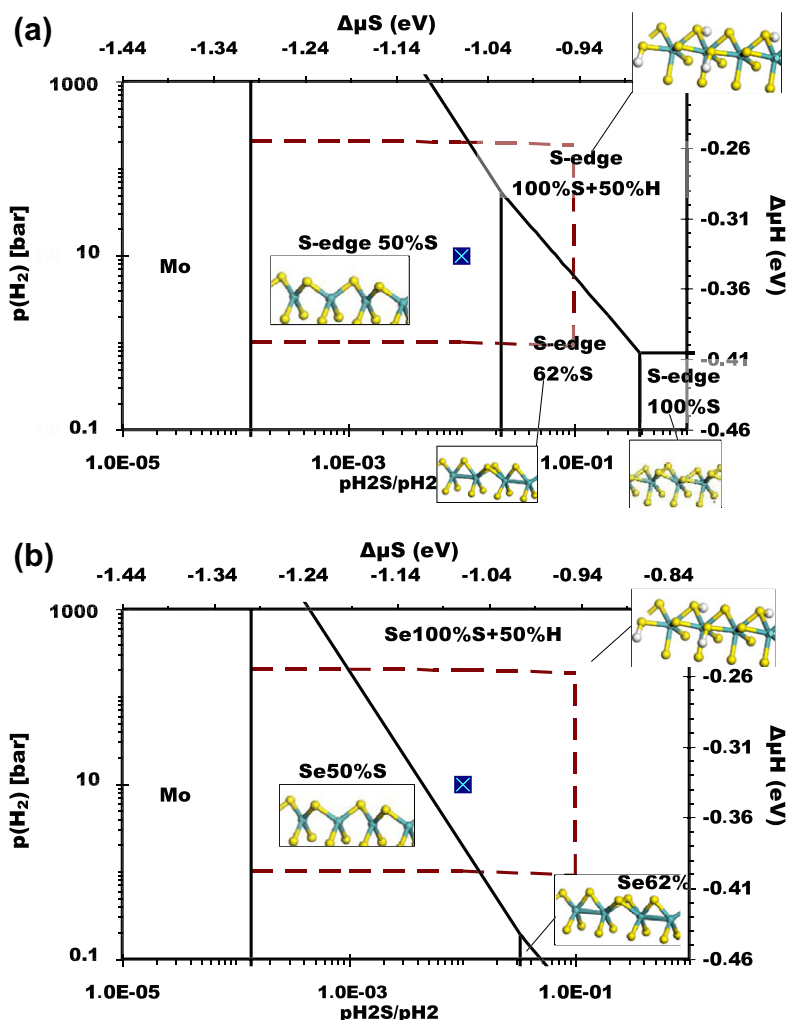


Fig. 12. (a) Phase diagram of the S-edge at 623 K according to the H_2 pressure and to the $p(\text{H}_2\text{S})/p(\text{H}_2)$ ratio. The state Se100%S + 50%H is represented as Fig. 5b, and the state Se62%S as Fig. 5c. The brown dashed lines represents the boundary conditions of HDS, a total pressure of 1 bar, a total pressure of 200 bars and a 10% $p(\text{H}_2\text{S})/p(\text{H}_2)$ ratio. The assumed HDS conditions (10 bar of H_2 pressure and $p(\text{H}_2\text{S})/p(\text{H}_2)$ ratio of 0.1) by Bollinger et al. [17,18] are represented by the crossed square dot. (b) Same as (a) but without including thermal and entropic corrections on surface states energies.

be due to the harmonic model or to the finite difference step size (in our case 0.02 \AA) used to compute the Hessian Matrix. The uncertainty on this last parameter for our system was estimated at most to be 20 cm^{-1} (step size between 0.01 \AA and 0.02 \AA) for real frequencies, so it should not be solely responsible for the discrepancy. The interaction between hydrogens for the S4_bis state affects the vibration frequencies, especially for the vibration along the axis formed by the two hydrogens, which corresponds to the lowest S–H bending frequency (496 and 505 cm^{-1}). On the M-edge 50%S, the diffusion barriers for surface hydrogen atoms are low, so it is expected that H diffusion occurs on the edge surface. Then, for larger distances between H ad-atoms, and therefore reduced interaction, the predicted vibration will be closer to the experimental value. Whatever the bending vibration frequencies, the experimental data bring out the stability of hydrogen on the edges in the following conditions $T = 473 \text{ K}$, $p(\text{H}_2) = 1, 20, \text{ or } 50 \text{ bar}$, and a 10% $p(\text{H}_2\text{S})/p(\text{H}_2)$ ratio, which is in agreement with our phase diagram Fig. 13b (S-edge 100%S + 50%H) and Fig. 13a (M-edge 50%S + 50%H, S4_bis) for both edges.

Moreover, we have identified, e.g. for state S2, vibrations of Mo–H groups ranging between 1800 cm^{-1} and 1900 cm^{-1} . A similar mode was only observed and assigned for metal hydride/sulfur complexes by Burrow et al. [44], but was never observed, as far as we know, on MoS_2 -based catalysts. Since S2 is never a predicted

stable state in usual conditions of observation, this lack of occurrence supports the higher stability of the S–H bond compared to the Mo–H bond, as predicted from our phase diagrams. The other situation for which we find a Mo–H bond is S25 (S-edge 50%S + 25%H), which is not a stable state according to our prediction. For the stretching mode of this bond, we predict frequencies 1294 cm^{-1} and 1370 cm^{-1} . These frequencies have never been observed experimentally, in agreement with our stability prediction.

From this analysis, we conclude that our computational predictions are in good agreement with the vibrational spectroscopy data released so far. We did not find contradictions from this rather stringent test of theoretical results.

3.4. Brønsted–Evans–Polanyi relationships (BEPR)

Since a lot of activation barriers for adsorption and desorption processes have been brought out along this study, it is interesting to explore if Brønsted–Evans–Polanyi relationships (BEPR) may exist. It is worth to mention that when a BEPR exists for a direct reaction step, another BEPR can be derived for the reverse reaction. Given $E_{a,d}$ the activation energy for the direct process and ΔE_d the corresponding reaction energy, the BEPR states that:

$$E_{a,d} = \lambda E_d + \beta \quad (8)$$

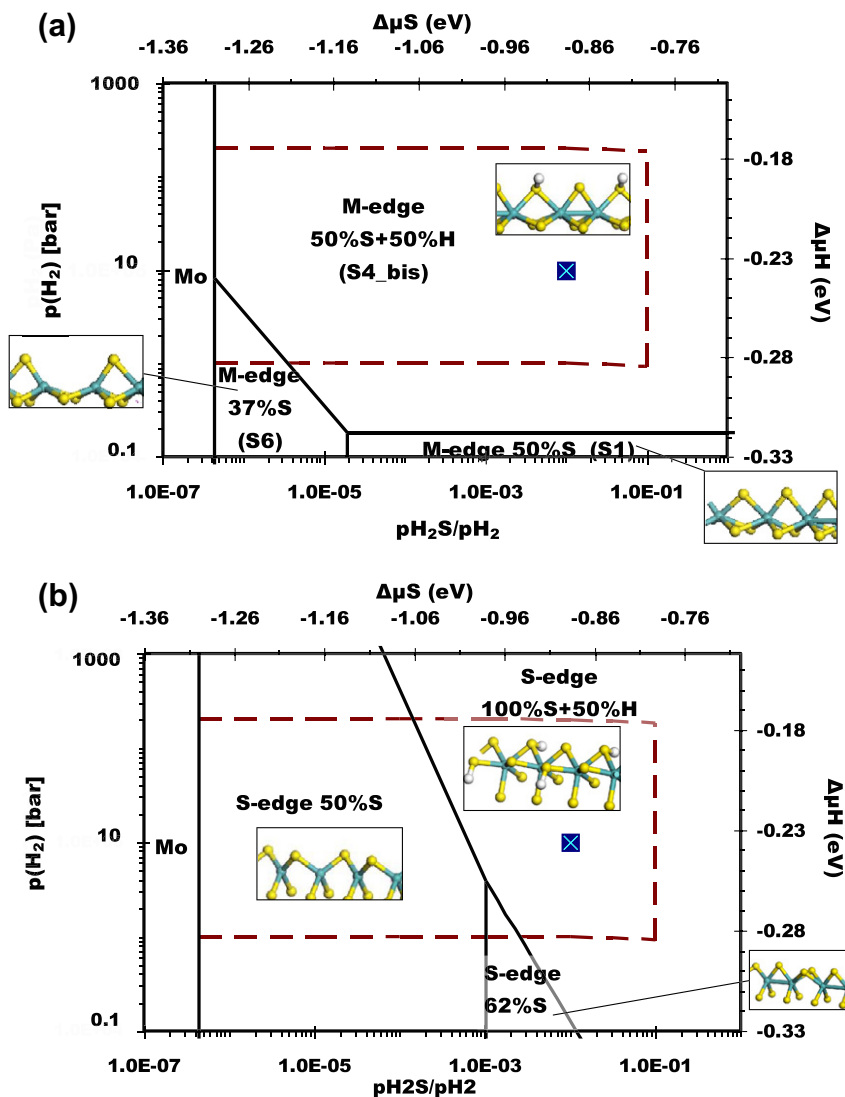


Fig. 13. M-edge and S-edge phase diagrams at 473 K (a and b), 573 K (c and d). As in Figs. 11 and 12, the dashed brown lines represent the HDS boundary conditions (total pressure between 1 and 200 bars, and maximum $p(\text{H}_2\text{S})/p(\text{H}_2)$ ratio 0.2). The assumed HDS conditions (10 bar of H_2 pressure and $p(\text{H}_2\text{S})/(\text{H}_2)$ ratio of 0.1) by Bollinger et al. [17,18] are represented by the crossed square dots.

For the reverse reaction, due to energy conservation, $\Delta E_r = -\Delta E_d$, and $Ea_r = Ea_d + \Delta E_r = Ea_d - \Delta E_d$; therefore, one obtains:

$$Ea_r = (1 - \lambda)\Delta E_r + \beta \quad (9)$$

So knowing the equation for one reaction, we can easily find the equation for the reverse reaction.

As presented in Fig. 14, relatively good correlations are obtained for H_2 and H_2S associative desorptions, supporting the existence of BEPR for such processes and their reverses.

We should mention that for diffusion processes, despite the fact that all the barriers were calculated along reaction pathways, no clear BEPR was found. This is due to the dependency of the activation energy on several parameters during diffusion processes. In particular, the bond strength and the bond stretching before creation of another bond are responsible for the location of the transition state (TS) along the reaction pathway (determining an early or late transition state [45]). Besides, the edge structure relaxation, and the repulsive interaction between hydrogens will affect the activation energy.

3.4.1. Associative desorption of H_2

For such processes, the relation between activation energy and reaction energy is well described by the BEPR straight line except for two outliers at $\Delta E = -0.24$ eV and $\Delta E = 0.12$ eV. These 2 points correspond respectively to the reverses of homolytic dissociation on S-edge 50%S and heterolytic dissociation on M-edge 50%S. It has been shown in the recent work of Van Santen et al. [45] that the BEPR depends on the site where the reaction occurs.

In our case, the associative desorption reaction on the M-edge related to one of these outliers involves one molybdenum and one sulfur (heterosynthetic: $\text{S}_2\text{-S}_1$ via TS1, see Fig. 2) unlike other associative desorptions on the M-edge, where desorption involves two sulfurs (homosynthetic). Lower stretching frequencies of Mo–H bonds with respect to S–H bonds (see Table 3) already reflect a lower (restoring) force constant in the first case (weaker local curvature of the potential energy surface), while the opposite partial charges borne by hydrogens (Mo– $\text{H}^{\delta-}$ and S– $\text{H}^{\delta+}$) are also in favor of the observed lower activation energy for heterosynthetic association at comparable energy of reaction.

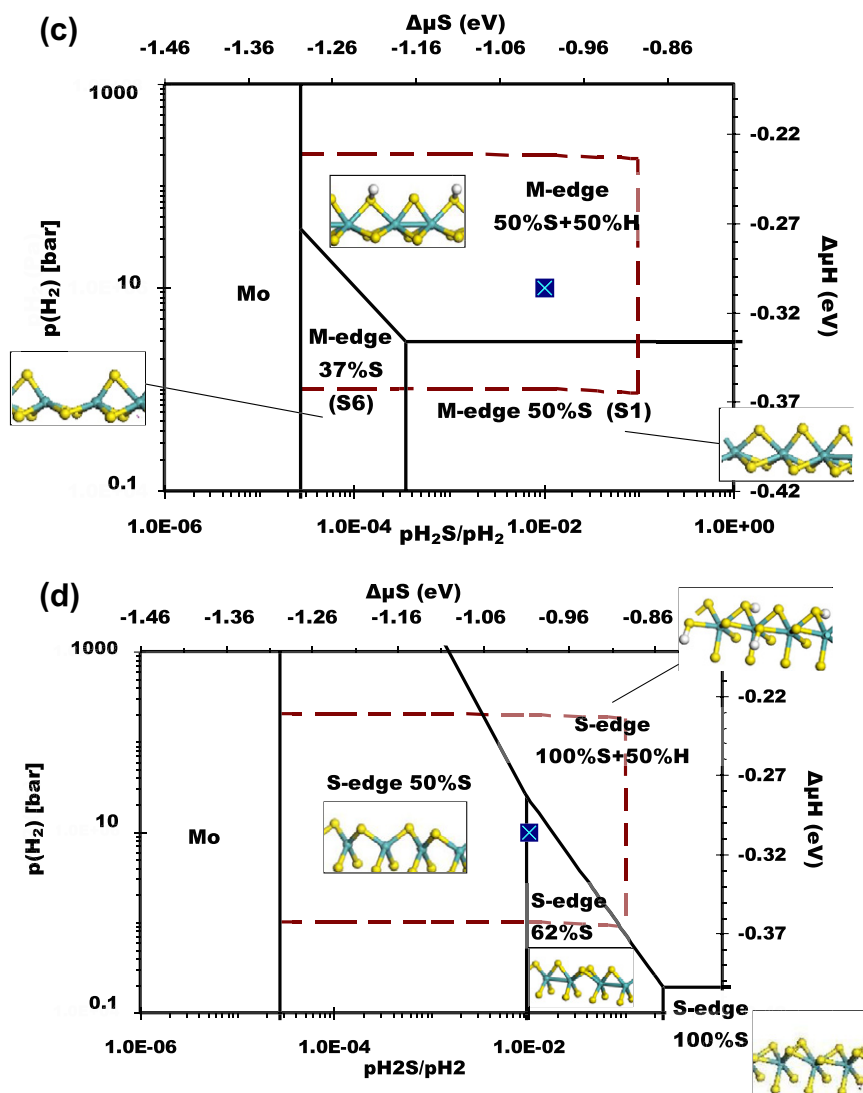


Fig. 13 (continued)

Concerning the homosynthetic associative desorption of H_2 from the S-edge 50%S, the main difference with other homosynthetic associations on the S-edge is the lower coordination of Mo atoms, which tends to localize more electronic density on terminal S atoms. According to the Bader analysis [28,29] of the electronic density of the atoms on the hydrogen-free edges, Table 2, the total charge on the S atom is $-0.96e$ for the S-edge 50%S (S21 in Fig. 7), whereas on the S-edge 100%S (S2 in Fig. 4a), the total charge on the separated sulfur atoms is $-0.78e$. At the transition states (TS21 for S-edge 50%S, Fig. 7, and TS2 for S-edge 100%S, Fig. 4a), the total charges on the sulfur atoms are $-0.76e$ and $-0.62e$ for S-edge 50%S and S-edge 100%S respectively. During the process of associative desorption, the dominantly ionic S–H bond is stretched, but the attractive (mostly electrostatic) interaction between hydrogen and sulfur is larger for S-edge 50%S since more charge resides on sulfur. Hereby, the bonding between sulfur and hydrogen is less extended, resulting in a TS state with a shorter S–H bond (1.58 \AA on the S-edge 50%S versus 1.79 \AA on the S-edge 100%S). This effect is responsible for a larger H–H distance at the TS state (1.11 \AA for the S-edge 50%S versus 0.92 \AA for the S-edge 100%S). This difference in the H–H distance reflects a 0.75 eV increase in the binding energy of H_2 at the TS on S-edge 100%S versus S-edge 50%S.

Accordingly, the activation of H_2 homosynthetic associative desorption is less favoured on S-edge 50%S than predicted by the BEPR which holds for homosynthetic associative desorption on S-edge 100%.

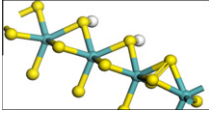
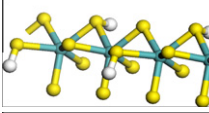
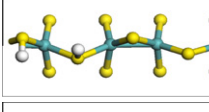
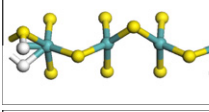
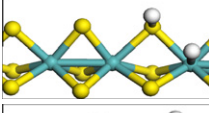
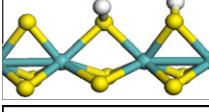
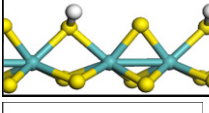
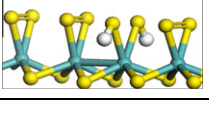
In the case of the heterosynthetic associative desorption from molybdenum and sulfur on the S-edge 50%S (S25–S26 via TS25, Fig. 8, $\Delta E = 0.35 \text{ eV}$, barrier 0.97 eV), the two effects counteract (more attraction of $\text{H}^{\delta+}$ by $\text{S}^{\delta-}$, less attraction of $\text{H}^{\delta-}$ by $\text{Mo}^{\delta+}$), and the BEPR main tendency is followed again.

3.4.2. Desorption of H_2S

It is worth to notice that in order to check whether a BEPR exists, it is necessary to take into account the energy of elementary processes, as stated by Van Santen et al. [45] as well as the energies of transition state and pre-transition state. The change of activation energy for desorption of H_2S as function of the reaction energy is well described by a BEPR very close to the main diagonal ($\lambda = 1$, $\beta = 0$) except for one value which corresponds to the homosynthetic associative desorption of H_2S from the M-edge 100%S (data from [4]). The pre-transition state corresponds then to two SH groups bonded to the same Mo and interacting through a $\text{H} \cdots \text{SH}$ hydrogen bond. For the other H_2S desorption processes considered either on

Table 3

Comparison of the experimental and theoretical normal modes. (1) Corresponds to Inelastic Neutron Scattering (INS) experiments by Sundberg et al. [42], (2) to Raman spectroscopy experiments by Polz et al. [41], and (3) to Infra-Red spectroscopy experiments by Burrow et al. [44].

Reference	S–H	S–S	Mo–H	Experimental conditions/model
Sundberg et al. (1) INS	2500(s) 650(b)			$T = 573$ K under $p(\text{H}_2\text{S})/p(\text{H}_2) = 10\%$, then $T = 473$ K under H_2 gas (1, 20, 50 bar)
Polz et al. (2) Raman Burrow et al. (3) IR spectroscopy		529(s)	1740(s) 1858(s)	$T = 573$ K; $p(\text{H}_2) = 300\text{--}450$ mbar; $p(\text{H}_2\text{S})/p(\text{H}_2) = 1/9 \Leftrightarrow \Delta\mu_{\text{S}} = -0.89$ eV $\text{Mo}(\text{H})(\text{tipt})_3(\text{PMe}_2\text{Ph})_2$ $\text{Mo}(\text{H})(\text{tipt})_3(\text{PEtPh}_2)$ $p = 1$ bar, $T = 293$ K
This work Se100%S	2598, 2591 (s) 685, 664 (b) 655, 653 (b)	536 (s)		 S5g
	2520, 2517(s) 676–658(b)			 100%S + 50%H
Se50%S	2582, 2524(s) 631, 574 (b) 542, 442 (b)			 S22
	2531 (s)		1374, 1285(s)	 S25
Me50%S	2587 (s) 662, 519 (b)		1871 (s) 736, 617 (b)	 S2
	2583, 2570(s) 639, 561 (b) 532, 489 (b)			 S4
	2573, 2567(s) 644, 640 (b) 505, 496 (b)			 S4_bis
Me100%S	2590, 2586(s) 624, 609 (b) 511, 506 (b)	576 (s)		 100%S + 25%H

the M-edge 50% or S-edge, the pre-transition state is always molecularly chemisorbed H_2S , bonded to one (top) or two (bridging) Mo ions. The associative process precursor to molecularly chemisorbed H_2S is now the limiting step for the overall associative desorption, in particular for a process with a low desorption energy as S6–S7 (Fig. 4a) on the S-edge 100%S and S14–S15 (Fig. 6) on the S-edge 87%S.

One would have expected that the desorption energy should be inversely proportional to the S coverage, since as mentioned in Section 3.1.2.1.3, the S bond energy is inversely proportional to the S coverage. But since the associative desorption may be decomposed into an associative pre-process and a desorption process, the latter is associated to the former, and there is no rule of proportionality between S coverage and the H_2S desorption energy itself.

Considering all points including outliers, the BEPR straight lines for H_2 and H_2S desorption are rather parallel (slopes are almost the same 0.79 and 0.83); however, the activation energy for H_2 desorption is always higher than the activation energy for H_2S desorption. This means that, if we consider dissociative adsorption and associative desorption on the same site, when the binding energy of

sulfur on the edge is lower than ~ 0.8 eV (0.88/0.79–0.22/0.83), then the desorption of H_2S is faster than that of H_2 .

4. Discussion

4.1. Comparison with previously proposed surface phase diagrams for MoS_2 catalytic edges

The phase diagram at 623 K for the M-edge presented in Fig. 11 modifies the stability domains of hydrogen previously determined by Cristol et al. [15]. In agreement with Bollinger et al. and Lauritsen et al. [17,18], the stability of H on the edges is expected to be extended to less reducing conditions ($P(\text{H}_2)=5$ bars corresponding to $\Delta\mu_{\text{H}} = -0.35$ eV). Then, in contrast to Cristol and Bollinger, the stability domain of the Mo-edge at 50% sulfur coverage is surrounded by Mo-edge 50%S + 50%H and Mo-edge 37% S for $\frac{p(\text{H}_2\text{S})}{p(\text{H}_2)} = 10^{-3}$ (corresponding to $\Delta\mu_{\text{S}} = -1.2$ eV). Those states are stable in relevant HDS conditions since they are overlapped by the domain of relevant HDS conditions delimited by the dashed lines.

At this point, it is important to underline the significance of including thermal and entropic corrections in surface phase

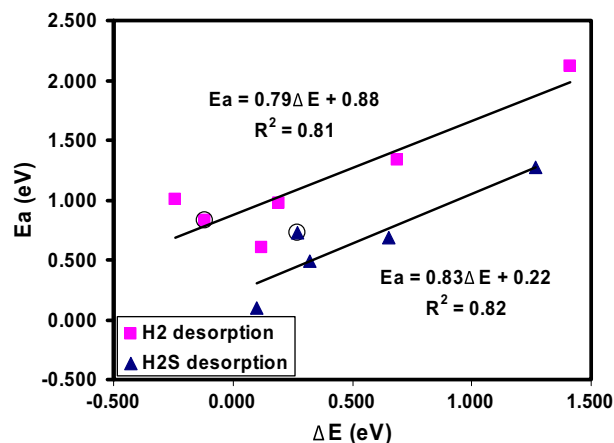


Fig. 14. Activation energies versus reaction energies for H_2 and H_2S associative desorption processes. A BEPR is brought out for each process. The squared coefficient of correlation is indicated below each regression line equation. All the values come from our present results except for one value (circled point) on each set of values coming from Mo-edge 100%S from Dinter et al. [4].

diagrams: the comparison of Figs. 11a and b, and 12a and b, is illustrative, showing that in relevant HDS conditions, the correct stable states may be missed out without such corrections.

4.2. Significance of our results with respect to the activation of dihydrogen by MoS_2 based HDS catalysts

In Section 3.1 were reported the activation energies for the heterolytic dissociative adsorption of H_2 on the M-edge 50%S (0.48 eV) and on the S-edge 50%S (0.62 eV), and the activation energies for the homolytic adsorption on the M-edge 100%S (0.95 eV) [4], S-edge 50%S (1.25 eV), and S-edge 100%S (0.65 eV). The phase diagram reported by Schweiger et al. [39] showed that S-edge and Mo-edge are in competition to determine the morphology of catalytic nanoparticles. The lowest activation energy is the one for the M-edge 50%S, and it has been shown on Fig. 11 that the resulting hydrogenated edge (M-edge 50%S + 50%H) may coexist with the 37%S hydrogen-free M-edge. Knowing the relative free energies of these states, it is possible to evaluate the fraction of sulfur vacancies at bridge sites of the M-edge 50%S + 50%H (S4-bis) (or fraction of M-edge 37%S). Starting from 100% of lacunar M-edge bridge sites at 575 K under 10 bar H_2 below 10^{-3} bar H_2S , this coverage decreases to 0.15% under 0.1 bar H_2S , but increases again to ca. 2% if temperature is then raised to 675 K. The M-edge 37%S should favor the chemisorption at the anionic vacancies, of the sulfur adatom from thiophenic derivatives present in crude oil fractions. Subsequently, hydrogens ad-atoms on the same edge are expected to be responsible for the hydrogenation and hydrodesulfuration of chemisorbed thiophenic derivatives.

On the S-edge 50%S, H_2 heterolytic dissociative adsorption subsequent to physisorption is exothermic but endergonic. On this same edge, H_2S associative desorption is the slowest process compared to that occurring on all other edges. Nevertheless, this does not mean that this edge does not play a role during HDS, since it is stable in relevant HDS conditions (see Figs. 12a and 13a and c) and sulfur adsorption should occur, as the activation energy for H_2S adsorption is expected to be around 0.1 eV. This value is calculated from the BEPR established in Section 3.4 with the energy difference:

$$\Delta E = (E_{\text{Me}50\%S} + E_{\text{H}_2\text{S}}) - E_{\text{E}62\%S+\text{H}}$$

where $E_{\text{E}62\%S+\text{H}}$ is the hydrogenated S-edge 62%S DFT energy, $E_{\text{Me}50\%S}$ is the DFT energy of the S-edge 50%S free of H, and $E_{\text{H}_2\text{S}}$

the DFT energy of H_2S in gas phase. This edge could also enable the adsorption of a thiophenic derivative if the steric effects are not too large.

The emerging picture for the lower ratios $p(\text{H}_2\text{S})/p(\text{H}_2)$ inside the range of relevant HDS conditions (left part of the dashed rectangles in Figs. 11–13) is then a situation where activated hydrogen is provided by the M-edge, while anionic vacancies are abundant on the S-edge, and scarce on the M-edge. The chemisorption of thiophenic compounds should be possible on these vacancies, but in strong competition with H_2S .

For higher ratios $p(\text{H}_2\text{S})/p(\text{H}_2)$ inside the range of relevant HDS conditions (right part of the dashed rectangles in Figs. 11–13), and for instance with reference to the conditions 10 bar of H_2 pressure and $p(\text{H}_2\text{S})/p(\text{H}_2)$ ratio of 0.1 brought forward by Bollinger et al. [17], [18], and represented by the crossed square dots in Figs. 11–13, the situation changes somewhat. The stable edge surfaces of MoS_2 , upon spanning the relevant range of from lower to higher operating temperatures (475–700 K), are M-edge 50%S + 50%H (S4_bis) together with S-edge 100%S + 50%H at 475 K, then M-edge 50%S + 50%H (S4_bis) together with S-edge 62%S at 575 K, then M-edge 50%S + 50%H (S4_bis) together with S-edge 50%S at 623 K. In other terms, H_2 is dissociatively activated on both edges at the lower temperature, and as temperature increases, it remains available on the M-edge only, while being depleted from the S-edge, which also loses sulfur, offering more and more anionic vacancies. Still for these conditions, but above 648 K, the stable M-edge will become S1 (M-edge 50%S) also depleted in H; it then questionable whether MoS_2 will retain any catalytic activity in hydrogenation and/or hydrogenolysis. The stability of M-edge 50%S + 50%H will be of course recovered, and therefore the activity, likely, if $p(\text{H}_2)$ is increased beyond some threshold, the higher the operating temperature.

5. Conclusions

In this work, we have investigated a set of various reaction pathways for H_2S and H_2 dissociative adsorption and associative desorption, as well as various hydrogen diffusion processes occurring at both sulfur and molybdenum edges of MoS_2 , in conditions encompassing those of industrial hydrotreating.

For the first time in this context, DFT computations have been carried out for this system including thermal and entropic effects of the gas phase and catalytic edges. It has been shown that these effects have a significant impact on the activation free energies and on stabilities of intermediate states, hereby on and surface phase diagrams and transition kinetics.

In relevant HDS conditions, thermodynamically stable chemisorbed H states have been brought out on the M-edge 50%S and the S-edge 100%S. On the latter, for instance, at 623 K, the hydrogenated edge is stable for $p(\text{H}_2\text{S})/p(\text{H}_2)$ ratios above 0.01. On the former, for instance, the hydrogenated edge is stable beyond 5 bar of H_2 pressure and $p(\text{H}_2\text{S})/p(\text{H}_2) = 0.001$. On the latter, at 623 K and $p(\text{H}_2) = 5$ bar, the hydrogenated edge becomes stable only above $p(\text{H}_2\text{S})/p(\text{H}_2) = 0.03$. Moreover, it has been shown that the domains of stability of these hydrogenated edges extends to lower H_2 pressures and lower $p(\text{H}_2\text{S})/p(\text{H}_2)$ ratios when temperature decreases.

The possible coexistence of the hydrogenated M-edge 50%S (Me50%S + 50%H) and of the M-edge 50%S containing an anion vacancy (Me37S) has been evidenced. When for instance 100% of M-edge bridge sites is lacunar at 575 K under 10 bar H_2 below 10^{-3} bar H_2S , this coverage decreases to 0.15% under 0.1 bar H_2S , or ca. 2% at 675 K. These sulfur vacancies, although scarce on the M-edge, are abundant on the S-edge, and are expected to play an important role in the catalysis of hydrodesulfuration reactions in the presence of un-promoted MoS_2 .

Since the hydrogenated S-edges 50%S + (50–100%H) are not thermodynamically stable according to the phase diagram, it should be interesting to verify to which extent they can show up as metastable states.

A comparison between experimental measurements reported in the literature, and our theoretical calculations of vibration frequencies allowed to identify S–H stretching and bending, and S–S stretching modes respectively at 2500, 650 and 530 cm^{-1} , belonging to surface species at both edges. The calculated vibration frequencies corresponding to the theoretically predicted stable surface species at conditions of measurements for the available spectroscopic experiments in literature are in agreement with the observed frequencies.

Several activation energies for H_2 dissociative adsorption have been computed for the main edges present in the relevant HDS conditions, i.e. S-edge 100%S, S-edge 50%S, and M-edge 50%S. The lowest barrier has been found for the H_2 dissociative adsorption process on the M-edge 50%S (0.48 eV). On the other edges, the barriers are slightly higher, with 0.65 or 0.86 eV and 0.78 eV respectively for S-edge 100% S starting from “separated” or “dimerized” S_2 bridge and S-edge 50%S.

The preferred pathways for dissociative association of H_2 are heterolytic on the M-edge 50%S, and S-edge 50%S, and homolytic on the S-edge 100%S, 87% S and generally as long as S_2 dimers are attacked.

The activation energies for H_2S associative desorption have been also computed for S-edge 100%S, S-edge 50%S and M-edge 50%S respectively at 2.07, 2.51 and 1.92 eV. Vibrational entropic corrections up to 0.6 eV depending on temperature have to be taken into account for estimates of free-energy barriers.

Two Brønsted–Evans–Polanyi Relationships have been determined for the associative desorption of H_2 and H_2S , and outliers to these BEPR have been discussed.

We think that this work provides a well quantified determination of the chemical active species at the edges of the MoS_2 nano-crystallites in HDS conditions. A great attention was paid to provide the stability domains of CUS, sulfhydryl group, sulfur anions as a function of temperature and partial pressures of H_2S , H_2 . Moreover, the kinetic properties of these species were also evaluated: hydrogen dissociative adsorption, hydrogen diffusion, and CUS creation associated to H_2S desorption. We hope that this will help for a more accurate investigation of the elementary steps of HDS mechanisms where the same active species are involved.

Finally, the question remains open of the influence of kinetics on the edges meta-stabilities. However, in view of the large number of interacting processes involved, and in order to gather statistically meaningful data over large enough time lags and site numbers, we expect first-principles based kinetic Monte Carlo simulations to be an efficient approach to address these questions. Considering such perspectives, we hope that the present work provides an appropriately extensive database of DFT barriers, complementing consistently our previous contributions [3,32].

Acknowledgments

This work has been performed within the SIRE Project (Grant No. ANR-06-CIS6-014-04) sponsored by the Agence Nationale de la Recherche (ANR).

Appendix A. Supplementary material

Supplementary data associated with this article can be found, in the online version, at doi:10.1016/j.jcat.2011.03.017.

References

- [1] P. Raybaud, Appl. Catal. A: Gen. 322 (2007) 76.
- [2] J.F. Paul, S. Cristol, E. Payen, Catal. Today 130 (2008) 139.
- [3] P.G. Moses, B. Hinneemann, H. Topsøe, J.K. Nørskov, J. Catal. 268 (2009) 201.
- [4] N. Dinter, M. Rusanen, P. Raybaud, S. Kasztelan, P. da Silva, H. Toulhoat, J. Catal. 267 (2009) 67.
- [5] H. Topsøe, B.S. Clausen, Catal. Rev. Sci. Eng. 26 (1984) 395.
- [6] S. Kasztelan, D. Guillaume, Ind. Eng. Chem. Res. 33 (1994) 203.
- [7] S. Kasztelan, H. Toulhoat, J. Grimblot, J.P. Bonnelle, Appl. Catal. 13 (1984) 127.
- [8] A. Travert, H. Nakamura, R. Van Santen, S. Cristol, J. Paul, E. Payen, J.A.C.S. 124 (2002) 7084.
- [9] J.F. Paul, E. Payen, J. Phys. Chem. B 107 (2003) 4057.
- [10] M. Sun, A.E. Nelson, J. Adjaye, Catal. Today 105 (2005) 36.
- [11] P.G. Moses, B. Hinneemann, H. Topsøe, J.K. Nørskov, J. Catal. 248 (2007) 188.
- [12] R.J.H. Voorhoeve, J.C.M. Stuijver, J. Catal. 23 (1971) 243.
- [13] A. Vambeke, L. Jalowiecki, J. Grimblot, J.P. Bonnelle, J. Catal. 109 (1988) 320.
- [14] L.S. Byskov, J.K. Nørskov, B.S. Clausen, H. Topsøe, J. Catal. 187 (1999) 109.
- [15] S. Cristol, J.F. Paul, E. Payen, D. Bougeard, S. Clemendot, F. Hutschka, J. Phys. Chem. B 106 (2002) 5659.
- [16] M. Sun, A.E. Nelson, J. Adjaye, J. Catal. 233 (2005) 411.
- [17] M.V. Bollinger, K.W. Jacobsen, J.K. Nørskov, Phys. Rev. B 67 (2003) 85410.
- [18] J.V. Lauritsen, M.V. Bollinger, E. Lægsgaard, K.W. Jacobsen, J.K. Nørskov, B.S. Clausen, H. Topsøe, F. Besenbacher, J. Catal. 221 (2004) 510.
- [19] W. Kohn, L.J. Sham, Phys. Rev. 140 (1965) A1133.
- [20] G. Kresse, J. Furthmüller, Comput. Mater. Sci. 6 (1996) 15.
- [21] J.P. Perdew, J.A. Chevary, S.H. Vosko, K.A. Jackson, M.R. Pederson, D.J. Singh, C. Fiolhais, Phys. Rev. B 46 (1992) 6671.
- [22] J.P. Perdew, Y. Wang, Phys. Rev. B 45 (1992) 13244.
- [23] G. Kresse, D. Joubert, Phys. Rev. B 59 (1999) 1758.
- [24] H.J. Monkhorst, J.D. Pack, Phys. Rev. B 13 (1976) 5188.
- [25] H. Jónsson, G. Mills, K.W. Jacobsen, in: B.J. Berne, G. Ciccotti, D.F. Coker, (Eds.), Classical and Quantum Dynamics in Condensed Phase Simulations, World Scientific, Singapore, 1998, p. 385.
- [26] G. Henkelman, B.P. Uberuaga, H. Jónsson, J. Chem. Phys. 113 (2000) 9901.
- [27] G. Henkelman, H. Jónsson, J. Phys. Chem 111 (1999) 7010.
- [28] R.F.W. Bader, Atoms in Molecules – A Quantum Theory, Oxford University Press, Oxford, 1990.
- [29] G. Henkelman, A. Arnaldsson, H. Jónsson, Comput. Mater. Sci. 36 (2006) 254.
- [30] E. Sanville, S.D. Kenny, R. Smith, G. Henkelman, J. Comput. Chem. 28 (2007) 899.
- [31] W. Tang, E. Sanville, G. Henkelman, J. Phys.: Comp. Mater. 21 (2009) 084204.
- [32] N. Dinter, M. Rusanen, P. Raybaud, S. Kasztelan, P. da Silva, H. Toulhoat, J. Catal. 275 (2010) 117.
- [33] R.A. van Santen, J.W. Niemantsverdriet, Chemical Kinetics and Catalysis, Plenum Press, New York, 1995.
- [34] P. Raybaud, J. Hafner, G. Kresse, S. Kasztelan, H. Toulhoat, J. Catal. 189 (2000) 129.
- [35] G. Soave, Chem. Eng. Sci. 27(1972) 1197.
- [36] P. Raybaud, J. Hafner, G. Kresse, H. Toulhoat, Phys. Rev. Lett. 80 (1998) 1481.
- [37] P. Raybaud, H. Toulhoat, J. Hafner, G. Kresse, in: B. Delmond, J.F. Froment, P. Grange, (Eds.), Proceedings of the 2nd International Symposium on Hydrotreatment and Hydrocracking of Oil Fractions, Studies in Surface Science and Catalysis, vol. 127, 1999, pp. 309–317.
- [38] B. Hinneemann, J.K. Nørskov, H. Topsøe, J. Phys. Chem. B 109 (2005) 2245.
- [39] H. Schweiger, P. Raybaud, G. Kresse, H. Toulhoat, J. Catal. 207 (2002) 76.
- [40] E. Krebs, B. Silvi, P. Raybaud, Catal. Today 130 (2008) 160–169.
- [41] J. Polz, H. Zeilinger, B. Müller, H. Knözinger, J. Catal. 120 (1989) 22–28.
- [42] P. Sundberg, R.B. Moyes, J. Tomkinson, Bull. Soc. Chim. Belg. 100 (1991) 967.
- [43] J.A. Spirko, M.L. Neiman, A.M. Oelker, K. Klier, Surf. Sci. 572 (2004) 191.
- [44] T.E. Burrow, N.J. Lazarowych, R.H. Morris, J. Lane, R.L. Richards, Polyhedron 8 (1989) 1701.
- [45] R.A. Van Santen, M. Neurock, S.G. Shetty, Chem. Rev. 110–114 (2010) 2005.